FINITE VOLUME EVOLUTION GALERKIN (FVEG) METHODS FOR HYPERBOLIC SYSTEMS

M. LUKÁČOVÁ - MEDVIĎOVÁ*, K.W. MORTON†, AND G. WARNECKE‡

Abstract. The subject of the paper is the derivation and analysis of new multidimensional, high-resolution, finite volume evolution Galerkin (FVEG) schemes for systems of nonlinear hyperbolic conservation laws. Our approach couples a finite volume formulation with approximate evolution operators. The latter are constructed using the bicharacteristics of the multidimensional hyperbolic system, such that all of the infinitely many directions of wave propagation are taken into account. In particular, we propose a new FVEG-scheme, which is designed in such a way that for a linear wave equation system the approximate evolution operator calculates any one-dimensional planar wave exactly. This operator improves the stability of the FVEG-scheme considerably leading to a stability limit closer to 1. Using the results obtained for the wave equation system a new approximate evolution operator for the linearised Euler equations is also derived. The integrals over the cell interfaces also need to be approximated with care; in this case our choice of Simpson's rule is guided by stability analysis of model problems. Second order resolution is obtained by means of a piecewise bilinear recovery. Numerical experiments confirm the accuracy and multidimensional behaviour of the new scheme.

Key words: genuinely multidimensional schemes, hyperbolic systems, wave equation, Euler equations, finite volume methods, evolution Galerkin schemes

AMS Subject Classification: 35L05, 65M06, 35L45, 35L65, 65M25, 65M15

1. Introduction. We consider the initial value problem for systems of hyperbolic conservation laws

$$\begin{aligned} &\boldsymbol{u}_t + \operatorname{div} \mathcal{F}(\boldsymbol{u}) = 0, \quad \boldsymbol{u}(\boldsymbol{x},t) \,:\, \mathbb{R}^d \times \mathbb{R}^+ \to \mathbb{R}^m, \\ &\boldsymbol{u}(\boldsymbol{x},0) = \boldsymbol{u}_0(\boldsymbol{x}). \end{aligned} \tag{1.1}$$

In particular, we present methods for the two-dimensional Euler equations of compressible fluid flows. As a first step in the exposition we treat their linearized form at zero advection velocity as in [8]. Application of the ideas to the three-dimensional case follows naturally, but though it is more straightforward (because of the odd number of dimensions) it is more technical, see e.g. Zahaykah [20]; and the incorporation of boundary conditions for initial-boundary value problems is also achieved in a natural way.

In general, finite volume methods are of two types: residual distribution (or fluctuation splitting) schemes were developed by Deconinck, Struijs, and Roe in [4] for steady hyperbolic problems and are most approriate for near-steady situations; while those derived from evolution Galerkin or semi-Lagrangian methods are our preference in cases where the evolutionary behaviour is most important. Our concern here is solely with the second class of methods and this paper forms a natural development from two earlier papers—Morton [18] which considered FVEG methods for scalar problems, and Lukáčová *et al.* [8] which introduced the approximate evolution operators we shall use here. For the use of the one-dimensional Riemann solvers for multidimensional problems see the wave propagation algorithm of LeVeque [6], and the more general presentation in [7].

*Arbeitsbereich Mathematik, Technische Universität Hamburg-Harburg, Germany (lukacova@tu-harburg.de).

†Bath and Oxford Universities, United Kingdom (Bill.Morton@comlab.ox.ac.uk).

‡Institut für Analysis und Numerik, Universität Magdeburg, Germany (Gerald.Warnecke@mathematik.uni-magdeburg.de).

Let Ω be our computational domain. We consider a general mesh for Ω with mesh size parameter $h > 0$. Suppose that S_h^p and S_h^r are finite element spaces consisting of piecewise polynomials of degrees $r \geq p \geq 0$. Let $\boldsymbol{U}^n$ be an approximation in the space S_h^p to the exact solution $\boldsymbol{u}(\cdot, t_n)$ at a time $t_n > 0$ and take $E_\tau : S_h^r \to X$ to be a suitable approximation to the exact evolution operator $E(\tau)$, $\tau > 0$, where X is a suitable function space for (1.1). We denote by $P_h : X \to S_h^p$ the L^2-projection onto S_h^p and by $R_h : S_h^p \to S_h^r$ a recovery operator introduced to give a higher order accuracy than that provided by S_h^p. Then an evolution Galerkin method can be written in the equivalent forms

$$\boldsymbol{U}^{n+1} = P_h E_\Delta R_h \boldsymbol{U}^n \quad \text{or} \quad (R_h \boldsymbol{U}^{n+1}) = R_h P_h E_\Delta (R_h \boldsymbol{U}^n), \tag{1.2}$$

where the second form is used in the error analysis, see [17].
In [8] we presented first order schemes of this form for hyperbolic systems in two space dimensions. No recovery from the space of piecewise constants was considered, i.e. $p = 0$ and $R_h = Id$. First order approximations E_Δ to the evolution operator were used on the piecewise constant data. Here we shall develop new approximate evolution operators and use them in a finite volume framework. This allows second order methods to be based on the first order evolution operators, after an appropriate recovery stage has been introduced.
If $\boldsymbol{U}_i^n$ is an approximation to the average of $\boldsymbol{u}(\boldsymbol{x}, t_n)$ over a cell Ω_i of measure $|\Omega_i|$, then our schemes will be of the form

$$|\Omega_i|(\boldsymbol{U}_i^{n+1} - \boldsymbol{U}_i^n) + \Delta t \int_{\partial\Omega_i} \boldsymbol{n} \cdot \mathcal{F}(\boldsymbol{U}^{n+\frac{1}{2}}) \mathrm{d}S = 0, \tag{1.3}$$

where $\boldsymbol{U}^{n+\frac{1}{2}}$ is generated from a, possibly recovered, approximation $R_h \boldsymbol{U}^n$ which has been evolved to $t_n + \frac{1}{2}\Delta t$. This formula was obtained by integration of (1.1) over $(t_n, t_n + \Delta t) \times \Omega_i$ and use of the Gauss theorem as well as the midpoint rule in time on the flux term.
The approximate evolution will be accomplished through bicharacteristic cones constructed at quadrature points chosen for the integration of the fluxes over the cell faces; in the simplest cases these will be just the vertices of the mesh, but we shall see that this is not always appropriate. Hence a higher order algorithm consists of three steps: recovery of a higher order approximation $R_h \boldsymbol{U}^n$ from the cell averages $\{\boldsymbol{U}_i^n\}$; approximate evolution to $t_n + \frac{1}{2}\Delta t$ to calculate the fluxes; and then an update of the cell averages by (1.3).
Such an algorithm is closely related to two-step versions of the Lax-Wendroff method; in particular, the advantages of the so-called rotated-Richtmyer form, in which the fluxes are approximated by applying the trapezoidal rule to updated quantities at the vertices, have been pointed out by Morton and Roe [19]. On a uniform square mesh this scheme will therefore be taken as a yardstick for our numerical comparisons; and it will also provide a guide to the analysis of stability. Thus on a general two-dimensional mesh, if we use the trapezoidal rule for the flux integrals and use a cyclic notation $\{\alpha\}$ to label the vertices of a polygonal cell Ω_i, the update equation that includes this Lax-Wendroff method and some of our FVEG schemes becomes

$$\begin{aligned} |\Omega_i|(\boldsymbol{U}_i^{n+1} - \boldsymbol{U}_i^n) + \tfrac{1}{2}\Delta t \sum_\alpha \Big\{ &[\boldsymbol{F}_1(\boldsymbol{U}_{\alpha+1}^{n+\frac{1}{2}}) + \boldsymbol{F}_1(\boldsymbol{U}_\alpha^{n+\frac{1}{2}})][y_{\alpha+1} - y_\alpha] \\ &- [\boldsymbol{F}_2(\boldsymbol{U}_{\alpha+1}^{n+\frac{1}{2}}) + \boldsymbol{F}_2(\boldsymbol{U}_\alpha^{n+\frac{1}{2}})][x_{\alpha+1} - x_\alpha] \Big\} = 0, \end{aligned} \tag{1.4}$$

where we have written $(\boldsymbol{F}_1, \boldsymbol{F}_2)$ for the $\mathcal{F}$ of (1.3).
However, we shall show that in general it is preferable to use Simpson's rule for the integrals of the fluxes along the cell edges. Its advantages for the scalar advection equation are easily demonstrated, and these are carried over to the system wave equation with advection, and to the Euler equations. The stability analysis used here, and in the selection of approximate evolution operators, has been based on a combination of energy analysis, Fourier analysis and maximum principles, followed up by extensive numerical validation. Details of the analysis will be presented elsewhere, in order to limit the length of the present paper.
The layout of the paper is as follows. Its core is formed by the next section, together with the appendix, where we will derive the approximate evolution operators to be used later: Section 2.1 gives the general formulae on the bicharacteristic cones obtained by quasi-diagonalising the locally frozen Jacobian matrices; then these are applied to the system wave equation in Section 2.2, giving exact integral equations for the solution; and in Sections 2.3 and 2.4 the approximate, explicit, evolution operators to be used in Section 3.1 are derived—for piecewise constant and continuous bilinear data respectively. The key idea here is to exploit the fact that an explicit solution to the wave equation is available for one-dimensional data, and to make the formulae exact for such cases. In Section 3 we first describe the discontinuous bilinear recovery scheme that is preferred, and give the reasoning for selecting Simpson's rule for edge integrals of the fluxes; then the proposed FVEG schemes are derived for the wave equation and Euler system—in Sections 3.3 and 3.4 respectively. Finally, in Section 4 numerical results are presented to show the superior stability and accuracy of the proposed FVEG schemes as compared with the natural alternatives considered during their derivation.

2. Approximate evolution operators. The distinctive feature of our proposed methods is the use of approximate evolution operators in the calculation of the fluxes $\boldsymbol{F}_1$ and $\boldsymbol{F}_2$. So we first describe a general approach to the derivation of the exact evolution operator for any constant coefficient first order hyperbolic system and point out the role of the bicharacteristics.

2.1. General formulae. Consider a general hyperbolic system in d space dimensions

$$\boldsymbol{u}_t + \sum_{k=1}^{d} \mathcal{A}_k \boldsymbol{u}_{x_k} = 0, \;\; \boldsymbol{x} = (x_1, \ldots, x_d)^T \in \mathbb{R}^d, \tag{2.1}$$

where the coefficient matrices $\mathcal{A}_k, k = 1, \ldots, d$ are in $\mathbb{R}^{m\times m}$ and the dependent variables are $\boldsymbol{u} = (u_1, \ldots, u_m)^T \in \mathbb{R}^m$. Because of the assumed hyperbolicity of the system we have m real eigenvalues $\lambda_j, j = 1, \ldots, m$ and corresponding linearly independent right eigenvectors $\boldsymbol{r}_j = \boldsymbol{r}_j(\boldsymbol{n})$, $j = 1, \ldots, m$ of the matrix pencil $\mathcal{A}(\boldsymbol{n}) := \sum_{k=1}^{d} n_k \mathcal{A}_k$ for any unit vector $\boldsymbol{n} = (n_1, \ldots, n_d)^T \in \mathbb{R}^d$. Since a common factor is irrelevant we assume $|\boldsymbol{n}| = 1$. In the case $d = 2$ we replace $\boldsymbol{n}$ on the unit circle by $(\cos\theta, \sin\theta)$, $\theta \in [0, 2\pi[$.
We denote by $\mathcal{R} = \mathcal{R}(\boldsymbol{n}) := (\boldsymbol{r}_1, \ldots, \boldsymbol{r}_m)$ the matrix of the right column eigenvectors. For any direction $\boldsymbol{n}$ the characteristic variables $\boldsymbol{w} = \boldsymbol{w}(\boldsymbol{n}) = (w_1, \ldots, w_m)^T$ for a general, possibly nonlinear, hyperbolic system, are defined by $\partial \boldsymbol{w}(\boldsymbol{n}) = \mathcal{R}^{-1}(\boldsymbol{n}) \partial \boldsymbol{u}$, i.e. for constant coefficient matrices this can be integrated to yield $\boldsymbol{w} = \mathcal{R}^{-1}\boldsymbol{u}$, $\boldsymbol{u} = \mathcal{R}\,\boldsymbol{w}$. Multiplying (2.1) by $\mathcal{R}^{-1}$ from the left we obtain the system in characteristic

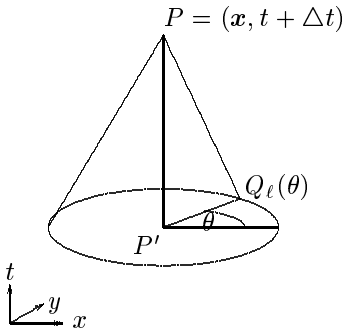

FIG. 2.1. *Bicharacteristic along the Mach cone through P and $Q_\ell(\theta)$.*

variables

$$\boldsymbol{w}_t + \sum_{k=1}^{d} \mathcal{B}_k \boldsymbol{w}_{x_k} = 0 \tag{2.2}$$

where $\mathcal{B}_k := \mathcal{R}^{-1}\mathcal{A}_k\mathcal{R} = (b_{ij}^k)_{i,j=1}^m$. We introduce the decomposition $\mathcal{B}_k = \mathcal{D}_k + \mathcal{B}_k'$, where $\mathcal{D}_k$ is the matrix containing the diagonal part of $\mathcal{B}_k$. This gives a quasi-diagonalised system

$$\boldsymbol{w}_t + \sum_{k=1}^{d} \mathcal{D}_k \boldsymbol{w}_{x_k} = -\sum_{k=1}^{d} \mathcal{B}_k' \boldsymbol{w}_{x_k} =: \boldsymbol{S}, \tag{2.3}$$

The ℓ-th bicharacteristic corresponding to the ℓ-th equation of the system (2.3) is defined by

$$\frac{\mathrm{d}\boldsymbol{x}_\ell}{\mathrm{d}t} = \boldsymbol{b}_{\ell\ell}(\boldsymbol{n}) := (b_{\ell\ell}^1, \ldots, b_{\ell\ell}^d)^T, \tag{2.4}$$

where $b_{\ell\ell}^k$ is the x_k component of the ℓ-th characteristic velocity, the so-called ray velocity, see [3] or [5]. We integrate the ℓ-th equation of the system (2.3) from the point P down to the point $Q_\ell(\boldsymbol{n})$, where the bicharacteristic hits the plane through P'. This situation is depicted in Figure 1 for a special case. Note that in general the set traced out by $Q_\ell(\boldsymbol{n})$ can be quite complicated, see Courant and Hilbert [3, pp. 599-618]. For a linear constant coefficient problem this will be a straight line. In this case $\mathcal{A}(\boldsymbol{n})$ is constant. For a nonlinear system we have to linearize by freezing the Jacobian matrices $\mathcal{A}_k(\boldsymbol{u})$ at a suitable state $\bar{\boldsymbol{u}}$. Thus, without lost of generality we assume in what follows that $\mathcal{A}(\bar{\boldsymbol{u}}, \boldsymbol{n})$ is constant.
Integration along the bicharacteristics introduces a formula for the characteristic variables

$$w_\ell(P, \boldsymbol{n}) - w_\ell(Q_\ell(\boldsymbol{n}), \boldsymbol{n}) = S_\ell'(\boldsymbol{n}), \;\; \ell = 1, \ldots, m, \tag{2.5}$$

with $S_\ell'(\boldsymbol{n}) = \int_t^{t+\triangle t} S_\ell(\boldsymbol{x}_\ell(\tilde{t}, \boldsymbol{n}), \boldsymbol{n}, \tilde{t})\, \mathrm{d}\tilde{t}$. This is already an exact integral representation of the solution at a new time step $t + \Delta t$. By multiplication of (2.5) by $\mathcal{R}$ from the left and integration of the variable $\boldsymbol{n}$ over the unit sphere O in $\mathbb{R}^d$ we obtain the

exact integral equation in the original variables $\boldsymbol{u}$,

$$\begin{aligned} \boldsymbol{u}(P) = \boldsymbol{u}(\boldsymbol{x}, t+\triangle t) &= \frac{1}{|O|}\int_O \mathcal{R}(\boldsymbol{n}) \begin{bmatrix} w_1(Q_1(\boldsymbol{n}),\boldsymbol{n}) \\ \vdots \\ w_m(Q_m(\boldsymbol{n}),\boldsymbol{n}) \end{bmatrix} \mathrm{d}O + \tilde{\boldsymbol{S}} \\ &= \frac{1}{|O|}\int_O \sum_{j=1}^{m} w_j(Q_j(\boldsymbol{n}),\boldsymbol{n})\, \boldsymbol{r}_j(\boldsymbol{n})\, \mathrm{d}O + \tilde{\boldsymbol{S}} \end{aligned} \tag{2.6}$$

with

$$\tilde{\boldsymbol{S}} = (\tilde{S}_1, \ldots, \tilde{S}_m)^T := \frac{1}{|O|}\int_O \mathcal{R}(\boldsymbol{n})\, \boldsymbol{S}'(\boldsymbol{n})\, \mathrm{d}O = \frac{1}{|O|}\int_O \int_t^{t+\Delta t} \mathcal{R}(\boldsymbol{n})\, \boldsymbol{S}(\boldsymbol{n}, \tilde{t})\, \mathrm{d}\tilde{t}\, \mathrm{d}O.$$

This is an *exact implicit representation formula* for the evolution operator. The second term contains the integral between the two time levels t and $t+\Delta t$ which in general cannot be evaluated exactly; it is a *mantle integral* over the mantle of the characteristic cone. The main goal of this paper is to derive a suitable approximation of the source term integrals which will lead to a scheme whose stability limit is closed to a natural CFL limit of 1.

2.2. System wave equation. Let us now illustrate the above general procedure on the two-dimensional linear hyperbolic system of the wave equation. Application to a nonlinear system of the Euler equations will be done in Section 3.4. The wave equation system can be written in the following form

$$\boldsymbol{u}_t + \mathcal{A}_1 \boldsymbol{u}_x + \mathcal{A}_2 \boldsymbol{u}_y = 0, \quad \boldsymbol{x} = (x,y)^T \in \mathbb{R}^2, \tag{2.7}$$

where the, noncommuting, coefficient matrices $\mathcal{A}_1, \mathcal{A}_2 \in \mathbb{R}^{3\times 3}$ are defined by

$$\mathcal{A}_1 := \begin{pmatrix} 0 & c & 0 \\ c & 0 & 0 \\ 0 & 0 & 0 \end{pmatrix}, \quad \mathcal{A}_2 := \begin{pmatrix} 0 & 0 & c \\ 0 & 0 & 0 \\ c & 0 & 0 \end{pmatrix}.$$

Here $c \in \mathbb{R}$ denotes the speed of sound and $\boldsymbol{u} = (\phi, u, v)^T \in \mathbb{R}^3$ is the vector of dependent variables. We have three eigenvalues $\lambda_1 = -c, \lambda_2 = 0, \lambda_3 = c$ and corresponding linearly independent right eigenvectors

$$\boldsymbol{r}_1 = \begin{bmatrix} -1 \\ \cos\theta \\ \sin\theta \end{bmatrix}, \quad \boldsymbol{r}_2 = \begin{bmatrix} 0 \\ \sin\theta \\ -\cos\theta \end{bmatrix}, \quad \boldsymbol{r}_3 = \begin{bmatrix} 1 \\ \cos\theta \\ \sin\theta \end{bmatrix}$$

of the matrix pencil $\mathcal{A}(\boldsymbol{n}) := \mathcal{A}_1 \cos\theta + \mathcal{A}_2 \sin\theta$ for any unit vector $\boldsymbol{n} = (n_x, n_y)^T = (\cos\theta, \sin\theta)^T \in \mathbb{R}^2$. Repeating the above procedure for this particular system we end with the following exact integral equations for the solution of the wave equation

system (2.7), see also [8] for a detailed derivation: with $\tilde{t} = t + \Delta t - \tau$, we have

$$\phi(\boldsymbol{x}, t+\triangle t) = \frac{1}{2\pi}\int_0^{2\pi} [\phi(Q(\theta)) - u(Q(\theta))\ \cos\theta - v(Q(\theta))\ \sin\theta]\,\mathrm{d}\theta$$

$$-\frac{1}{2\pi}\int_0^{2\pi}\int_0^{\triangle t} S(\boldsymbol{x} + c\tau\boldsymbol{n}(\theta), \theta, \tilde{t})\,\mathrm{d}\tau\,\mathrm{d}\theta, \tag{2.8}$$

$$u(\boldsymbol{x}, t+\triangle t) = \frac{1}{2\pi}\int_0^{2\pi} [-\phi(Q(\theta))\ \cos\theta + u(Q(\theta))\ \cos^2\theta + v(Q(\theta))\ \sin\theta\ \cos\theta]\,\mathrm{d}\theta$$

$$+\frac{1}{2}u(P') + \frac{1}{2\pi}\int_0^{2\pi}\int_0^{\triangle t} \cos\theta S(\boldsymbol{x} + c\tau\boldsymbol{n}(\theta), \theta, \tilde{t})\,\mathrm{d}\tau\,\mathrm{d}\theta$$

$$-\frac{c}{2}\int_0^{\triangle t} \phi_x(P'(\tilde{t}))\,\mathrm{d}\tau, \tag{2.9}$$

$$v(\boldsymbol{x}, t+\triangle t) = \frac{1}{2\pi}\int_0^{2\pi} [-\phi(Q(\theta))\ \sin\theta + u(Q(\theta))\ \sin\theta\ \cos\theta + v(Q(\theta))\ \sin^2\theta]\,\mathrm{d}\theta$$

$$+\frac{1}{2}v(P') + \frac{1}{2\pi}\int_0^{2\pi}\int_0^{\triangle t} \sin\theta S(\boldsymbol{x} + c\tau\boldsymbol{n}(\theta), \theta, \tilde{t})\,\mathrm{d}\tau\,\mathrm{d}\theta$$

$$-\frac{c}{2}\int_0^{\triangle t} \phi_y(P'(\tilde{t}))\,\mathrm{d}\tau, \tag{2.10}$$

where the so-called source term S is given by

$$\begin{aligned} S(\tilde{\boldsymbol{x}}, \theta, \tilde{t}) := c[&u_x(\tilde{\boldsymbol{x}}, \theta, \tilde{t})\sin^2\theta \\ &- (u_y(\tilde{\boldsymbol{x}}, \theta, \tilde{t}) + v_x(\tilde{\boldsymbol{x}}, \theta, \tilde{t}))\sin\theta\cos\theta + v_y(\tilde{\boldsymbol{x}}, \theta, \tilde{t})\cos^2\theta], \end{aligned} \tag{2.11}$$

and $Q(\theta) = (x + c\Delta t\cos\theta, y + c\Delta t\sin\theta, t)$, $P' \equiv P'(t) = (x, y, t)$, $P'(\tilde{t}) = (x, y, \tilde{t})$.
Note that this form of the integral equations is not unique. There are other equivalent variations, see [8] for an example or (2.14) - (2.16). The difference plays a role in subsequent approximations where different forms of the integral equations may lead to different schemes. We have chosen to take the above formulation because it is the form that directly follows from the procedure described in Section 2.1.
A major drawback of the approximate evolution operators used for the EG schemes in [8] was that they did not provide full stability for a CFL number of 1, where we define CFL= $c\Delta t/h$. Since we had derived our approximate evolution operators from exact integral equations, the loss of stability was obviously due to the approximations we derived from the integral equations (2.8), (2.9) and (2.10). One of the steps was to use quadrature in time on the mantle integrals $\frac{1}{2\pi}\int_0^{2\pi}\int_0^{\Delta t}\mathrm{d}\tau\mathrm{d}\theta$ over the bicharacteristic

cones. In our first order EG schemes we were using piecewise constant data, in which case a discontinuity cuts through the cone mantle. The rectangle or the trapezoidal rule are not good quadrature rules for such discontinuous integrands.

From one dimensional advection on a uniform mesh we know that any scheme that is stable for CFL numbers up to 1 reproduces the exact solution to the advection problem in that limit, i.e. the data shifted by one mesh cell for CFL$=1$. We decided to look for correction terms to our approximate evolution operators by postulating the following design principle. Consider plane wave data parallel to one of the spatial axes. For a first order scheme these are taken as piecewise constant, i.e. quasi-one-dimensional Riemann data. Now we look for approximate evolution operators that reproduce the exact solution at the apex of the bicharacteristic cone centered at the original discontinuity. When considering slopes for second order schemes we devise approximate evolution operators for the slopes that again reproduce the solution for piecewise linear data exactly at the apex of the bicharacteristic cone centered at the kink or discontinuity of such data. The result is that we devise approximations to the mantle integrals that can be incorporated in the integrals around the cone base.

2.3. Piecewise constant data. Let us consider *first order schemes* and piecewise constant data first. Take the following plane wave, of Riemann problem type, as initial data for the wave equation system (2.7)

$$\begin{aligned}
\phi(x,y,0) &= \begin{cases} \phi^+ & x>0 \\ (\phi^+ + \phi^-)/2 & x=0 \\ \phi^- & x<0, \end{cases} \\
u(x,y,0) &= \begin{cases} u^+ & x>0 \\ (u^+ + u^-)/2 & x=0 \\ u^- & x<0, \end{cases} \\
v(x,y,0) &= 0.
\end{aligned} \tag{2.12}$$

The average value that we have accorded to $x=0$ will be used in formulae below. Then the exact solution at any time $t>0$ is given by

$$\begin{aligned}
\phi(x,y,t) &= \begin{cases} \phi^+ & x>ct \\ (\phi^+ + \phi^-)/2 - (u^+ - u^-)/2 & ct>x>-ct \\ \phi^- & x<-ct, \end{cases} \\
u(x,y,t) &= \begin{cases} u^+ & x>ct \\ (u^+ + u^-)/2 - (\phi^+ - \phi^-)/2 & ct>x>-ct \\ u^- & x<-ct, \end{cases} \\
v(x,y,t) &= 0.
\end{aligned} \tag{2.13}$$

An analogous solution for ϕ and v with $u=0$ may be considered for plane waves in $y-$direction. Due to obvious symmetry between u and v we do not need to work this out explicitly.

Let us now consider the integral equations (2.8), (2.9) and (2.10) as our starting point. To avoid the derivatives of the dependent variables appearing in S we may use Lemma 2.1 of [8] to convert these into a more convenient form involving the dependent variables themselves, see e.g. [8, (2.16)]. This gives us the following equivalent system of exact integral equations that we will normally use in all further considerations in

this paper. With $Q(\theta,\tilde{t}) = (x + c\tau\cos\theta, y + c\tau\sin\theta, \tilde{t})$, $\tilde{t} = t + \Delta t - \tau$,

$$\phi(\boldsymbol{x}, t+\triangle t) = \frac{1}{2\pi}\int_0^{2\pi} [\phi(Q(\theta)) - u(Q(\theta))\ \cos\theta - v(Q(\theta)\ \sin\theta)]\,\mathrm{d}\theta \tag{2.14}$$

$$-\frac{1}{2\pi}\int_0^{\triangle t}\frac{1}{\tau}\int_0^{2\pi}\left[u(Q(\theta,\tilde{t}))\ \cos\theta + v(Q(\theta,\tilde{t}))\ \sin\theta\right]\,\mathrm{d}\theta\,\mathrm{d}\tau,$$

$$u(\boldsymbol{x}, t+\triangle t) = \frac{1}{2\pi}\int_0^{2\pi}\left[-\phi(Q(\theta))\ \cos\theta + u(Q(\theta))\ \cos^2\theta + v(Q(\theta))\sin\theta\ \cos\theta\right]\,\mathrm{d}\theta$$

$$+\frac{1}{2}u(P') + \frac{1}{2\pi}\int_0^{\triangle t}\frac{1}{\tau}\int_0^{2\pi}\left[u(Q(\theta,\tilde{t}))\cos 2\theta\right. \tag{2.15}$$

$$\left.+v(Q(\theta,\tilde{t}))\sin 2\theta\right]\,\mathrm{d}\theta\,\mathrm{d}\tau - \frac{c}{2}\int_0^{\triangle t}\phi_x(P'(\tilde{t}))\,\mathrm{d}\tau,$$

$$v(\boldsymbol{x}, t+\triangle t) = \frac{1}{2\pi}\int_0^{2\pi}\left[-\phi(Q(\theta))\ \sin\theta + u(Q(\theta))\ \sin\theta\ \cos\theta + v(Q(\theta))\ \sin^2\theta\right]\,\mathrm{d}\theta$$

$$+\frac{1}{2}v(P') + \frac{1}{2\pi}\int_0^{\triangle t}\frac{1}{\tau}\int_0^{2\pi}\left[u(Q(\theta,\tilde{t}))\ \sin 2\theta\right. \tag{2.16}$$

$$\left.+v(Q(\theta,\tilde{t}))\ \cos 2\theta\right]\,\mathrm{d}\theta\,\mathrm{d}\tau - \frac{c}{2}\int_0^{\triangle t}\phi_y(P'(\tilde{t}))\,\mathrm{d}\tau.$$

To complete the elimination of derivatives we replace the terms in $\phi_x(P')$, $\phi_y(P')$ by their averages over the corresponding circular sections Ω_τ of the characteristic cone,

$$\phi_x(P'(\tilde{t})) \approx \frac{1}{\pi c^2\tau^2}\int_{\Omega_\tau}\phi_x\,\mathrm{d}x\mathrm{d}y = \frac{1}{\pi c\tau}\int_0^{2\pi}\phi(Q(\theta,\tilde{t}))\cos\theta\,\mathrm{d}\theta$$

so that we obtain

$$\frac{c}{2}\int_0^{\Delta t}\phi_x(P'(\tilde{t}))\,\mathrm{d}\tau \approx \frac{1}{2\pi}\int_0^{\Delta t}\frac{1}{\tau}\int_0^{2\pi}\phi(Q(\theta,\tilde{t}))\cos\theta\,\mathrm{d}\theta\mathrm{d}\tau, \tag{2.17}$$

with a similar expression for the ϕ_y term. Note that these are now in the same form as the other source term integrals in (2.14)-(2.16).
In the appendix these formulae are evaluated exactly for the one-dimensional solution (2.13) so that they yield the exact update from the data at $t = 0$ to the solution at $(0, 0, \Delta t)$. Moreover, they show how in this case the mantle integral can be combined with that round the cone base. From this result we propose the following approximate evolution operators for application to piecewise constant data on a general

two-dimensional mesh, on the design principle that it gives the exact result at the origin for the data of (2.12).

Approximate evolution operator E_Δ^{const} for *piecewise constant* functions:

$$\phi(P) = \frac{1}{2\pi}\int_0^{2\pi} [\phi(Q) - u(Q)\,\mathrm{sgn}(\cos\theta) - v(Q)\,\mathrm{sgn}(\sin\theta)\,]\,\mathrm{d}\theta, \tag{2.18}$$

$$u(P) = \frac{1}{2\pi}\int_0^{2\pi} \left[-\phi(Q)\,\mathrm{sgn}(\cos\theta) + u(Q)\left(\tfrac{1}{2} + \cos^2\theta\right) + v(Q)\,\sin\theta\,\cos\theta\right]\mathrm{d}\theta, \tag{2.19}$$

$$v(P) = \frac{1}{2\pi}\int_0^{2\pi} \left[-\phi(Q)\,\mathrm{sgn}(\sin\theta) + u(Q)\,\sin\theta\,\cos\theta + v(Q)\left(\tfrac{1}{2} + \sin^2\theta\right)\right]\mathrm{d}\theta, \tag{2.20}$$

where $Q = (x + c\Delta t\cos\theta, y + c\Delta t\sin\theta, t)$, $P' = (x, y, t)$, and $P = (x, y, t + \Delta t)$. Our choice seems to be the simplest approximation that produces the desired effect. Moreover we should point out that if $\nu = c\Delta t/h = 1$ the error of the above approximate evolution operator is $\mathcal{O}(\Delta t^2)$; otherwise the approximation error is $\mathcal{O}(\Delta t)$.

2.4. Continuous bilinear data. To obtain *second order schemes* we choose to use a bilinear recovery of the data, cf. (3.1, 3.2) for a precise definition. We now need an approximate evolution that incorporates the slopes ϕ_x, ϕ_y, ϕ_{xy}, u_x, etc. Let us consider the following initial data

$$\phi(x,y,0) = \begin{cases} \phi^R x & x > 0 \\ 0 & x \le 0, \end{cases} \qquad u(x,y,0) = \begin{cases} u^R x & x > 0 \\ 0 & x \le 0, \end{cases} \qquad v(x,y,0) = 0. \tag{2.21}$$

For simplicity we have taken the left state to be zero. Note that for the linear wave equation system the superposition principle holds and a more general piecewise linear solution can easily be deduced. The exact solution is given by

$$\begin{aligned} \phi(x,y,t) &= \begin{cases} \phi^R x - u^R ct & x > ct \\ \frac{1}{2}(\phi^R - u^R)(x + ct) & -ct < x \le ct \\ 0 & x \le -ct \end{cases} \\ u(x,y,0) &= \begin{cases} u^R x - \phi^R ct & x > ct \\ \frac{1}{2}(u^R - \phi^R)(x + ct) & -ct < x \le ct \\ 0 & x \le -ct \end{cases} \\ v(x,y,t) &= 0. \end{aligned} \tag{2.22}$$

The appendix gives the result of substituting these data into the mantle integrals of (2.14) -(2.17). As a result it is shown how the corresponding cone base integrals can be modified so as to incorporate the contributions from the mantle integrals, in such a way that the exact solution (2.22) is reproduced at $(0, 0, \Delta t)$. This leads to an approximate evolution operator E_Δ^{bilin} for *continuous piecewise bilinear data* which is given as follows:

$$\phi(P) = \phi(P') + \frac{1}{4}\int_0^{2\pi} [\phi(Q) - \phi(P')]\,\mathrm{d}\theta - \frac{1}{\pi}\int_0^{2\pi} [u(Q)\cos\theta + v(Q)\sin\theta]\,\mathrm{d}\theta + \mathcal{O}(\Delta t^2), \tag{2.23}$$

$$u(P) = u(P') - \frac{1}{\pi}\int_0^{2\pi} \phi(Q)\,\cos\theta\,\mathrm{d}\theta + \frac{1}{4}\int_0^{2\pi} \Big[3\,(u(Q)\cos\theta + v(Q)\sin\theta)\cos\theta - u(Q) - \tfrac{1}{2}u(P')\Big]\mathrm{d}\theta + \mathcal{O}(\Delta t^2), \tag{2.24}$$

$$v(P) = v(P') - \frac{1}{\pi}\int_0^{2\pi} \phi(Q)\,\sin\theta\,\mathrm{d}\theta + \frac{1}{4}\int_0^{2\pi} \Big[3\,(u(Q)\cos\theta + v(Q)\sin\theta)\,\sin\theta - v(Q) - \tfrac{1}{2}v(P')\Big]\mathrm{d}\theta + \mathcal{O}(\Delta t^2). \tag{2.25}$$

As indicated here, these formulae are generally only first order accurate; but they have been designed in such a way that they will be second order accurate for certain classes of data. In both this sub-section and the previous one, we have made use of the well established design principle of designing formulae which are exact for specific data with a finite number of degrees of freedom. Morever, note that the overall accuracy of the FVEG scheme is determined by the incorporation of these approximations in the FV update (1.3).

3. Second order schemes based on linear recovery.

3.1. Continuous and discontinuous bilinear recovery. On a general two-dimensional mesh, of triangles or quadrilaterals, a useful first step in the construction of more accurate approximations from cell averages is to recover values at each of the vertices of the mesh. Each vertex value is typically obtained as a mean of the cell averages from all the cells that share the vertex, see [18] for examples and further references. On a triangular mesh this leads immediately to a piecewise linear interpolatory approximation; on a quadrilateral mesh it again gives a continuous interpolatory approximation through the vertex values which is bilinear in the local variables on each quadrilateral (the so-called isoparametric bilinear approximation). Unfortunately, the cell averages are not preserved in either case. And even in a finite volume method, in which the recovered approximation is used only to calculate the fluxes through the cell boundaries, it is important to preserve the cell averages - what Barth calls *conservation in the mean*, see Barth [1] and Morton [18] for arguments making this point. The simplest way to retain this property is to add a constant to the approximation in each cell, so that it is now discontinuous across cell boundaries. We limit ourselves here to considering such recovery procedures in the case of a uniform square mesh, partly so that we can readily compare with alternative finite difference schemes. So we consider a regular mesh for our computational domain Ω, which consists of the square mesh cells $\Omega_{ij} \equiv [(i-\frac{1}{2})h, (i+\frac{1}{2})h] \times [(j-\frac{1}{2})h, (j+\frac{1}{2})h] = [x_{i-1/2}, x_{i+1/2}] \times [y_{j-1/2}, y_{j+1/2}] = [x_\alpha, x_{\alpha+1}] \times [y_\beta, y_{\beta+1}]$, where $i, j \in \mathbb{Z}$ are used to denote indices of mesh cells, $\alpha, \beta \in \mathbb{Z}$ are indices of vertices, and $h > 0$ is the mesh size parameter. We introduce the finite difference operators

$$\mu_x v(x) = \tfrac{1}{2}\,[v(x+h/2) + v(x-h/2)] \quad \text{and} \quad \delta_x v(x) = v(x+h/2) - v(x-h/2)$$

with an analogous notation for the y-direction. Then the recovery of the vertex values is expressed as $\tilde{\boldsymbol{U}} = \mu_x\mu_y\boldsymbol{U}$; with the parametrization just given this leads to

$$\tilde{\boldsymbol{U}}_{\alpha\beta} = \mu_x\mu_y\boldsymbol{U}_{i+1/2,j+1/2} \equiv \frac{1}{4}\left[\boldsymbol{U}_{i+1\,j+1} + \boldsymbol{U}_{i+1\,j} + \boldsymbol{U}_{i\,j+1} + \boldsymbol{U}_{ij}\right],$$

but it is often clearer to omit the subscripts which we shall do below when this is the case. Continuous bilinear recovery with these vertex values can be expressed directly in terms of the cell averages as

$$R_h^C\boldsymbol{U}\Big|_{\Omega_{ij}} = \Big(\mu_x^2\mu_y^2 + \frac{(x-x_i)}{h}\mu_x\mu_y^2\delta_x + \frac{(y-y_j)}{h}\mu_x^2\mu_y\delta_y + \frac{(x-x_i)(y-y_j)}{h^2}\mu_x\mu_y\delta_x\delta_y\Big)\boldsymbol{U}_{ij}. \quad (3.1)$$

To restore the cell averages we need a shift of $(1-\mu_x^2\mu_y^2)\boldsymbol{U}_{ij}$, or equivalently the use of the vertex values only to approximate the x-, y- and xy-derivatives, giving the conservative discontinuous bilinear recovery

$$R_h^D\boldsymbol{U}\Big|_{\Omega_{ij}} = \left(1 + \frac{(x-x_i)}{h}\mu_x\mu_y^2\delta_x + \frac{(y-y_j)}{h}\mu_x^2\mu_y\delta_y + \frac{(x-x_i)(y-y_j)}{h^2}\mu_x\mu_y\delta_x\delta_y\right)\boldsymbol{U}_{ij}. \quad (3.2)$$

We have studied both recoveries theoretically from the stability point of view, as well as experimentally. In the following we will use them to derive new second order FVEG methods.

3.2. Stability and the evaluation of edge fluxes. The key step in a finite volume method is the evaluation of the cell interface fluxes. By the use of the midpoint rule in (1.3) for the time integration, and by approximating the mantle integrals in the evolution operator of (2.8) - (2.10) by the cone base integrals of (2.18) - (2.20) and (2.23) - (2.25), we have reduced the four-dimensional flux integrals for the wave equation to just two dimensions. The integration along a cell edge we prefer to approximate by a suitable quadrature, for ease of generalization to the Euler equations. But the integral around the perimeter of the cone base we will evaluate exactly so as to pick up all characteristic directions.
The obvious quadrature points are vertices, used in the trapezoidal rule, and the midedge points used in the midpoint rule; in combination they give Simpson's rule. We have considered these three quadrature rules as alternatives to the exact evaluation of edge fluxes for both piecewise constant data and the continuous bilinear data given by the recovery R_h^C in (3.1). We know that for the wave equation the use of the trapezoidal rule has the special property of preserving a natural discrete measure of vorticity, see [19]. However, the Euler equations have advected Mach cones, see Figure 2, so that another natural test problem for our methods is the scalar two-dimensional advection equation

$$u_t + au_x + bu_y = 0, \quad (3.3)$$

where $a, b > 0$ are constant advection velocities. Now for (3.3) exact flux evaluation for piecewise constant data yields the FV-scheme

$$\begin{aligned} U_{ij}^{n+1} &= \left[1 - \nu_x\Delta_{-x}\left(1 - \tfrac{1}{2}\nu_y\Delta_{-y}\right) - \nu_y\Delta_{-y}\left(1 - \tfrac{1}{2}\nu_x\Delta_{-x}\right)\right]U_{ij}^n \quad (3.4)\\ &\equiv \left[1 - \nu_x\Delta_{-x}\right]\left[1 - \nu_y\Delta_{-y}\right]U_{ij}^n, \end{aligned}$$

where $\nu_x := a\Delta t/h$, $\nu_y := b\Delta t/h$, and the backward difference Δ_{-x} is defined as $\Delta_{-x}U_i := U_i - U_{i-1}$, with an analogous notation for the y-direction.
The scheme (3.4) is thus the tensor product of the one-dimensional upwind schemes and it is well-known that it is monotone and stable for $(\nu_x, \nu_y) \in [0,1] \times [0,1]$. Note too that this is normally derived by exact time integration of the fluxes, but with these data the same result is obtained by using the midpoint rule for the time integration. However, if we used the midpoint rule along the edge we would obtain the scheme

$$U_{ij}^{n+1} = [1 - \nu_x\Delta_{-x} - \nu_y\Delta_{-y}]\, U_{ij}^n, \tag{3.5}$$

which is stable only for $\nu_x + \nu_y \in [0,1]$. Worse still, the use of the trapezoidal rule for the edge integrals gives

$$U_{ij}^{n+1} = \left[1 - \nu_x\Delta_{-x}\left(1 - \tfrac{1}{2}\Delta_{-y}\right) - \nu_y\Delta_{-y}\left(1 - \tfrac{1}{2}\Delta_{-x}\right)\right] U_{ij}^n \tag{3.6}$$

and one can show that this is stable only if $\nu_x = \nu_y$!
On the other hand, combining (3.5) and (3.6) by using Simpson's rule for the edge integrals gives the scheme

$$U_{ij}^{n+1} = \left[1 - \nu_x\Delta_{-x}\left(1 - \tfrac{1}{6}\Delta_{-y}\right) - \nu_y\Delta_{-y}\left(1 - \tfrac{1}{6}\Delta_{-x}\right)\right] U_{ij}^n, \tag{3.7}$$

which is stable in a region of the (ν_x, ν_y)-plane that includes the line $\nu_x = \nu_y$ out to $\nu_x + \nu_y \leq 6/5$ and the axes out to $12/13$. (Stability analysis for the schemes discussed in this paper has been carried out by a combination of Fourier analysis and energy analysis and will be published elsewhere.) Extensive numerical testing of the stability and accuracy of the schemes based on Simpson's rule, some of which is reported in Section 4, has led us to adopt it as the standard means of implementing our FVEG schemes.
We note here that the precise definition of CFL number ν will vary according to the problem and the mesh, but in general it is based on forming the ratio of the domain of dependence of the differential equation to that of its discrete approximation, and then taking the d-th root of the result when the problem is in $\mathbb{R}^d$. In this way, saying that a scheme is stable up to CFL number 1.0 would roughly correspond to the well-known CFL condition being sufficient as well as necessary for stability.
When continuous bilinear recovery is used, stability restrictions depend much less on the quadrature rule used for the edge integrals. For example, the second order Lax-Wendroff (rotated-Richtmyer) scheme, studied in [19] for the wave equation, uses the trapezoidal rule as a key element in its design and takes the form

$$U_{ij}^{n+1} = \left[1 - \nu L_\Delta\left(\mu_x\mu_y - \tfrac{1}{2}L_\Delta\right)\right] U_{ij}^n, \tag{3.8}$$

where $\nu = \Delta t/h$ and L_Δ is a central difference approximation to the spatial differential operator. For the linear advection equation (3.3) we therefore substitute

$$L_\Delta = a\mu_y\delta_x + b\mu_x\delta_y \tag{3.9}$$

in (3.8). An energy analysis shows that this is stable for

$$\nu_x^2 + \nu_y^2 \leq 1;$$

this is practically quite acceptable but does not correspond to stability up to CFL number 1.0 on our definition above.

When applied to the wave equation the stability condition of the Lax-Wendroff scheme (3.8) is $c\Delta t/h \leq 1$ and the scheme has many similarities with our FVEG schemes, based on the approximate evolution operator (2.23) - (2.25) and the continuous bilinear recovery (3.1). So we have used it as a guide to the stability analysis of our schemes; and, in Section 4, we present numerical results to show that the use of Simpson's rule is as good as the trapezoidal rule in this case.

However, our numerical tests have shown that when the trapezoidal rule is used with discontinuous data for the wave equation system with constant, but different, advection velocities a, b strong oscillations appear in the numerical solutions; this does not occur with Simpson's rule.

In order to construct local Mach cones for general nonlinear systems we need to define the local velocity of the flow $(\bar{u}, \bar{v})$ as well as the local speed of sound $\bar{a}$. This local flow information can be computed, for example, by an averaging process. When the trapezoidal or Simpson's rule is used, we average over four cells adjacent to the vertex or over two cells adjacent to the midpoint, respectively. Another possibility to get the local flow states $\bar{u}, \bar{v}$ and $\bar{a}$ would be to use a predictor step, e.g. the Lax-Friedrichs or the Osher-Solomon method, in order to compute this auxiliary information. This gives us the desired local flow velocities, which are computed either at the midpoints of cell interfaces or at the vertices, depending on the integral evaluation. From experiments we observed that it is fully sufficient to use the simple averaging described above.

3.3. Wave equation system. In this section we will specify more precisely how to compute $\boldsymbol{U}^{n+1/2}$ in order to evaluate the fluxes in (1.3). In particular we consider the wave equation system (2.7) and write down the finite difference formulation of the approximate evolution operators (2.18) - (2.20), (2.23) - (2.25) when piecewise constant or continuous piecewise bilinear approximate functions are used, respectively.

First, let us consider the approximate evolution operator E_{Δ}^{const}, given by (2.18) - (2.20) operating on a piecewise constant approximation, i.e. we have $R_h = Id$. We denote the CFL number by $\nu = c\Delta t/h$. Then the exact evaluation of the edge integral (as well as the bicharacteristic cone integrals) yields, e.g. for the vertical edge, the following finite difference scheme for $E_{\Delta,edge}^{const}\boldsymbol{U}^n$

$$
\begin{aligned}
\Phi_{edge}^{n+1/2} &= \left(1 + \frac{\nu}{2\pi}\delta_y^2\right)\mu_x\Phi^n - \left(\frac{1}{2} + \frac{\nu}{4\pi}\delta_y^2\right)\delta_x U^n - \frac{\nu}{\pi}\mu_x\mu_y\delta_y V^n, \qquad (3.10)\\
U_{edge}^{n+1/2} &= \left(1 + \frac{5\nu}{12\pi}\delta_y^2\right)\mu_x U^n - \left(\frac{1}{2} + \frac{\nu}{4\pi}\delta_y^2\right)\delta_x\Phi^n + \frac{\nu}{6\pi}\mu_x\delta_x\delta_y V^n,\\
V_{edge}^{n+1/2} &= \left(1 + \frac{5\nu}{12\pi}\delta_y^2\right)\mu_x V^n - \frac{\nu}{\pi}\mu_x\mu_y\delta_y\Phi^n + \frac{\nu}{6\pi}\mu_y\delta_x\delta_y U^n.
\end{aligned}
$$

The equations for the horizontal edge follow from symmetry. In what follows we give for the sake of simplicity only equations for the first and second components Φ and U, respectively; equations for the third component V will be analogous to those for U.

Using quadrature rules, e.g. the trapezoidal or Simpson's rule, we need to evaluate $\boldsymbol{U}_{\alpha,\beta}^{n+1/2}$ at a vertex (α, β). After exact evaluation of the Mach cone integrals the finite

difference formulae for $E_\Delta^{const}\boldsymbol{U}^n$ at a vertex read

$$\begin{aligned}\Phi_{vertex}^{n+1/2} &= \mu_x\mu_y\Phi^n - \frac{1}{2}\mu_y\delta_x U^n - \frac{1}{2}\mu_x\delta_y V^n, \\ U_{vertex}^{n+1/2} &= \mu_x\mu_y U^n - \frac{1}{2}\mu_y\delta_x\Phi^n + \frac{1}{4\pi}\delta_x\delta_y V^n.\end{aligned} \tag{3.11}$$

Analogous formulae hold for midpoints of cell interfaces, e.g. on a vertical edge we have

$$\begin{aligned}\Phi_{midpt}^{n+1/2} &= \mu_x\Phi^n - \tfrac{1}{2}\delta_x U^n, \\ U_{midpt}^{n+1/2} &= \mu_x U^n - \tfrac{1}{2}\delta_x\Phi^n.\end{aligned} \tag{3.12}$$

Now let us consider continuous piecewise bilinear recovery R_h^C, cf. (3.1), which can be rewritten equivalently in the following way. For example, for the upper right cell corresponding to a vertex (α,β), i.e. that centred at $x_i = x_\alpha + h/2$, $y_j = y_\beta + h/2$, we have

$$R_h^C\boldsymbol{U}\Big|_{\Omega_{ij}} := \left(1 + \frac{x-x_\alpha}{h}\Delta_{+x} + \frac{y-y_\beta}{h}\Delta_{+y} + \frac{(x-x_\alpha)(y-y_\beta)}{h^2}\Delta_{+x}\Delta_{+y}\right)\boldsymbol{U}_{\alpha\beta},$$

where $\Delta_{+x}U_\alpha := U_{\alpha+1} - U_\alpha$ denotes the forward finite difference, and an analogous notation holds for the $y-$direction.
The finite difference formulation of the scheme

$$\boldsymbol{U}^{n+1/2} = E_\Delta^{bilin}R_h^C\boldsymbol{U}^n \tag{3.13}$$

then yields, after the exact evaluation of the integrals of (2.23) - (2.25) around the bicharacteristics cone,

$$\begin{aligned}\Phi_{vertex}^{n+1/2} = &\left(1 + \frac{\nu}{4}\delta_x^2 + \frac{\nu}{4}\delta_y^2 + \frac{\nu^2}{32}\delta_x^2\delta_y^2\right)\mu_x\mu_y\Phi^n \\ &-\frac{\nu}{2}\left(1 + \frac{\nu}{4\pi}\delta_y^2\right)\mu_x^2\mu_y\delta_x U^n - \frac{\nu}{2}\left(1 + \frac{\nu}{4\pi}\delta_x^2\right)\mu_x\mu_y^2\delta_y V^n,\end{aligned} \tag{3.14}$$

$$\begin{aligned}U_{vertex}^{n+1/2} = &\left(1 + \frac{\nu}{4}\delta_x^2 - \frac{\nu}{16}\delta_y^2 + \frac{\nu^2}{64}\delta_x^2\delta_y^2\right)\mu_x\mu_y U^n \\ &-\frac{\nu}{2}\left(1 + \frac{\nu}{4\pi}\delta_y^2\right)\mu_x^2\mu_y\delta_x\Phi^n + \frac{3\pi\nu^2}{64}\mu_x^2\mu_y^2\delta_x\delta_y V^n.\end{aligned}$$

In Section 4 we will present some numerical experiments for the FVEG scheme (1.3) where the value $\boldsymbol{U}^{n+1/2}$ is evolved by means of (3.14). Note that the recovery operator R_h^C in (3.13) does not preserve cell averages, which leads to reduced accuracy of this FVEG scheme, cf. scheme B in Table 1.
Therefore in order to maintain the cell averages at the recovery stage, by using $R_h^D = R_h^C + (1-\mu_x^2\mu_y^2)$ as given in (3.2), we propose the following EG operator. It combines approximate evolution (3.14), which is used to evolve slopes, with (3.11), which evolves the constant part:-

$$\boldsymbol{U}^{n+1/2} = E_\Delta^{bilin}R_h^C\boldsymbol{U}^n \;+\; E_\Delta^{const}(1-\mu_x^2\mu_y^2)\boldsymbol{U}^n. \tag{3.15}$$

Numerical experiments indicate that the above approximate evolution operator has stability limit close to the CFL number $\nu = 1$, and its accuracy is considerably better than that of (3.13).
Moreover, it is also easy to implement a limiting step, if it is required. Let $\Psi : \mathbb{R}^3 \to [0,1]$ be a limiter operator, then the approximate evolution operator for the second order FVEG scheme can be given in the following way

$$\boldsymbol{U}^{n+1/2} = E_\Delta^{const}\,\boldsymbol{U}^n \;+\; \left(E_\Delta^{bilin} R_h^C \mu_x^{-1}\mu_y^{-1} - E_\Delta^{const}\mu_x\mu_y\right)\,(\Psi\mu_x\mu_y\boldsymbol{U}^n)\,. \qquad (3.16)$$

Note that in the definition of R_h^C in (3.1) every term involves a $\mu_x\mu_y$ average, so the operator here merely removes this averaging step.
Due to its better properties we denote the scheme (3.15) as FVEG-A. We note that a separate evolution that incorporates the slopes has also been used by Ben-Artzi and Falcovitz [2] in their GRP method. The scheme (3.13) will be called FVEG-B. It is perhaps worth noting that if the operator E_Δ^{bilin} is applied directly to $R_h^D\boldsymbol{U}^n$, with $\boldsymbol{U}^n(P')$ interpreted as a local average, the resulting scheme is stable only to CFL numbers 0.6 or 0.8 according to whether Simpson's rule or the trapezoidal rule is used to approximate the edge integrals.

3.4. Euler equations. The finite volume formulation, which automatically implies conservation over the cell, works with the conservation form of the Euler equations

$$\boldsymbol{u}_t + \boldsymbol{F}_1(\boldsymbol{u})_x + \boldsymbol{F}_2(\boldsymbol{u})_y = 0, \qquad (3.17)$$

where the vector of conservative variables and the fluxes are

$$\boldsymbol{u} := \begin{pmatrix} \rho \\ \rho u \\ \rho v \\ e \end{pmatrix},\quad \boldsymbol{F}_1(\boldsymbol{u}) := \begin{pmatrix} \rho u \\ \rho u^2 + p \\ \rho uv \\ (e+p)u \end{pmatrix},\quad \boldsymbol{F}_2(\boldsymbol{u}) := \begin{pmatrix} \rho v \\ \rho uv \\ \rho v^2 + p \\ (e+p)v \end{pmatrix}.$$

Here ρ denotes the density, u and v components of velocity, p pressure, e total energy and γ stands for adiabatic exponent, $\gamma = 1.4$ for dry air. The state equation gives a relationship between the pressure and total energy, $e = p/(\gamma-1) + \rho(u^2+v^2)/2$. However, we have shown in [12] that in order to consider bicharacteristics and derive approximate evolution operators it is more appropriate to work with the simpler system in the primitive variables $\boldsymbol{v} = (\rho, u, v, p)$, namely

$$\boldsymbol{v}_t + \mathcal{A}_1(\boldsymbol{v})\boldsymbol{v}_x + \mathcal{A}_2(\boldsymbol{v})\boldsymbol{v}_y = 0, \quad \boldsymbol{x} = (x,y)^T \in \mathbb{R}^2, \qquad (3.18)$$

where

$$\boldsymbol{v} := \begin{pmatrix} \rho \\ u \\ v \\ p \end{pmatrix},\quad \mathcal{A}_1 := \begin{pmatrix} u & \rho & 0 & 0 \\ 0 & u & 0 & \frac{1}{\rho} \\ 0 & 0 & u & 0 \\ 0 & \gamma p & 0 & u \end{pmatrix},\quad \mathcal{A}_2 := \begin{pmatrix} v & 0 & \rho & 0 \\ 0 & v & 0 & 0 \\ 0 & 0 & v & \frac{1}{\rho} \\ 0 & 0 & \gamma p & v \end{pmatrix}.$$

This is the simplest and most convenient form for studying the bicharacteristics of the system away from shocks. To derive the integral equations we linearise system (3.18) by freezing the Jacobian matrices at a point $\bar{P} = (\bar{x}, \bar{y}, \bar{t})$. These points are chosen to be vertices or midpoints of cell interfaces depending on the quadrature rule used for

the flux integration along cell interfaces. Denote by $\bar{\boldsymbol{v}} = (\bar{\rho}, \bar{u}, \bar{v}, \bar{p})$ the local variables at the point $\bar{P}$ and by $\bar{a}$ the local speed of sound there, i.e. $\bar{a} = \sqrt{\gamma \bar{p}/\bar{\rho}}$. Thus the linearised system (3.18) with frozen constant coefficients has the form

$$\boldsymbol{v}_t + \mathcal{A}_1(\bar{\boldsymbol{v}})\boldsymbol{v}_x + \mathcal{A}_2(\bar{\boldsymbol{v}})\boldsymbol{v}_y = 0, \quad \boldsymbol{x} = (x, y)^T \in \mathbb{R}^2. \tag{3.19}$$

The eigenvalues of the matrix pencil $\mathcal{A}(\bar{\boldsymbol{v}}) = \mathcal{A}_1(\bar{\boldsymbol{v}})n_x + \mathcal{A}_2(\bar{\boldsymbol{v}})n_y$, where $\boldsymbol{n} = \boldsymbol{n}(\theta)$ $= (n_x, n_y)^T = (\cos\theta, \sin\theta)^T \in \mathbb{R}^2$, are

$$\begin{aligned}
\lambda_1 &= \bar{u}\,\cos\,\theta + \bar{v}\,\sin\,\theta - \bar{a} \\
\lambda_2 &= \lambda_3 = \bar{u}\,\cos\,\theta + \bar{v}\,\sin\,\theta \\
\lambda_4 &= \bar{u}\,\cos\,\theta + \bar{v}\,\sin\,\theta + \bar{a}.
\end{aligned}$$

Thus we have two simple eigenvalues, λ_1 and λ_4, which give genuinely nonlinear fields, i.e. acoustic or pressure waves; and two multiple eigenvalues, $\lambda_2 = \lambda_3$ associated with the entropy waves and vorticity waves, which are linearly degenerate. We can choose the following linearly independent right eigenvectors

$$\boldsymbol{r}_1 = \begin{pmatrix} -\frac{\bar{\rho}}{\bar{a}} \\ \cos\theta \\ \sin\theta \\ -\bar{\rho}\bar{a} \end{pmatrix}, \quad \boldsymbol{r}_2 = \begin{pmatrix} 1 \\ 0 \\ 0 \\ 0 \end{pmatrix}, \quad \boldsymbol{r}_3 = \begin{pmatrix} 0 \\ \sin\theta \\ -\cos\theta \\ 0 \end{pmatrix}, \quad \boldsymbol{r}_4 = \begin{pmatrix} \frac{\bar{\rho}}{\bar{a}} \\ \cos\theta \\ \sin\theta \\ \bar{\rho}\bar{a} \end{pmatrix}.$$

Let $\mathcal{R}(\bar{\boldsymbol{v}})$ be the matrix of the right eigenvectors and multiply system (3.19) by $\mathcal{R}^{-1}(\bar{\boldsymbol{v}})$ from the left. The quasi-diagonalised characteristic system of the linearised Euler equations has the following form

$$\boldsymbol{w}_t + \begin{pmatrix} \bar{u} - \bar{a}\cos\theta & 0 & 0 & 0 \\ 0 & \bar{u} & 0 & 0 \\ 0 & 0 & \bar{u} & 0 \\ 0 & 0 & 0 & \bar{u} + \bar{a}\cos\theta \end{pmatrix} \boldsymbol{w}_x + \begin{pmatrix} \bar{v} - \bar{a}\sin\theta & 0 & 0 & 0 \\ 0 & \bar{v} & 0 & 0 \\ 0 & 0 & \bar{v} & 0 \\ 0 & 0 & 0 & \bar{v} + \bar{a}\sin\theta \end{pmatrix} \boldsymbol{w}_y = \boldsymbol{S}, \tag{3.20}$$

where the vector $\boldsymbol{w}$ of characteristic variables reads

$$\boldsymbol{w} = \begin{pmatrix} w_1 \\ w_2 \\ w_3 \\ w_4 \end{pmatrix} = \mathcal{R}^{-1}(\bar{\boldsymbol{v}})\boldsymbol{v} = \begin{pmatrix} \frac{1}{2}(-\frac{p}{\bar{\rho}\bar{a}} + u\cos\theta + v\sin\theta) \\ \rho - \frac{p}{\bar{a}^2} \\ u\sin\theta - v\cos\theta \\ \frac{1}{2}(\frac{p}{\bar{\rho}\bar{a}} + u\cos\theta + v\sin\theta) \end{pmatrix},$$

and the right hand side is given as follows

$$\boldsymbol{S} = \begin{pmatrix} S_1 \\ S_2 \\ S_3 \\ S_4 \end{pmatrix} = \begin{pmatrix} \frac{1}{2}\bar{a}(\sin\theta\frac{\partial w_3}{\partial x} - \cos\theta\frac{\partial w_3}{\partial y}) \\ 0 \\ \bar{a}\sin\theta(\frac{\partial w_1}{\partial x} - \frac{\partial w_4}{\partial x}) - \bar{a}\cos\theta(\frac{\partial w_1}{\partial y} - \frac{\partial w_4}{\partial y}) \\ \frac{1}{2}\bar{a}(-\sin\theta\frac{\partial w_3}{\partial x} + \cos\theta\frac{\partial w_3}{\partial y}) \end{pmatrix}.$$

Note that it is the wave equation system which creates the key part of (3.20): suppose we set $\bar{\rho} = 1/\bar{a}$ and remove the first row corresponding to density as well as first column from the Jacobian matrices $\mathcal{A}_1, \mathcal{A}_2$ in (3.19); then moving the third equation for pressure to the first row leads to the so-called system wave equation with advection

$$\boldsymbol{u}_t + \mathcal{A}_1\boldsymbol{u}_x + \mathcal{A}_2\boldsymbol{u}_y = 0, \quad \boldsymbol{x} = (x, y)^T \in \mathbb{R}^2, \tag{3.21}$$

where $\boldsymbol{u} = (p, u, v)^T$ and

$$\mathcal{A}_1 := \begin{pmatrix} \bar{u} & \bar{a} & 0 \\ \bar{a} & \bar{u} & 0 \\ 0 & 0 & \bar{u} \end{pmatrix}, \quad \mathcal{A}_2 := \begin{pmatrix} \bar{v} & 0 & \bar{a} \\ 0 & \bar{v} & 0 \\ \bar{a} & 0 & \bar{v} \end{pmatrix}.$$

Further, if the advection velocities are $\bar{u} = \bar{v} = 0$ and $\bar{a} = const.$ we get the well-known linear wave equation system (2.7), which describes the propagation of acoustic waves. Note that in Section 2 as well as in [8] we did not consider advection terms, which are present in the linearised Euler equations system. These terms lead to more complex characteristic cone configurations that have to be taken into account in the implementation of the FVEG methods.

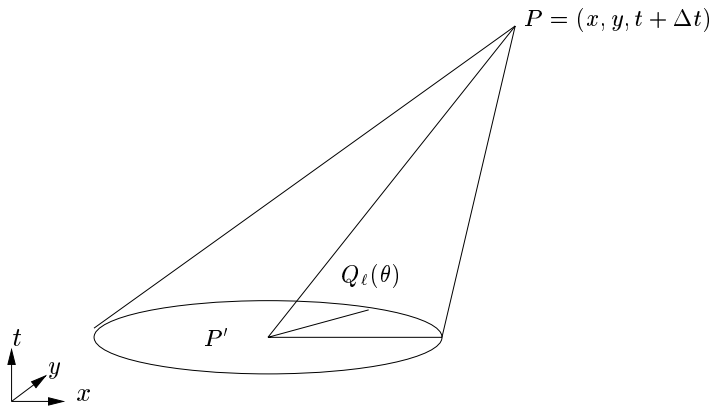

FIG. 3.1. *Bicharacteristics along the Mach cone through P and $Q_\ell(\theta)$.*

The approximate evolution operators for the Euler equations can be derived in an analogous way as in Section 2 for the wave equation system (2.7). The set of all bicharacteristics which connect the apex $P = (x, y, t + \Delta t)$ down to the footpoints $Q_\ell(\theta)$ creates the Mach cone shown in Figure 2. More precisely, the footpoints of the corresponding bicharacteristics are

$$\begin{aligned} Q_1(\theta) &= (x - (\bar{u} - \bar{a}\cos\theta)\Delta t, y - (\bar{v} - \bar{a}\sin\theta)\Delta t, t), \\ Q_2 &= Q_3 = (x - \bar{u}\triangle t, y - \bar{v}\Delta t, t), \\ Q_4(\theta) &= (x - (\bar{u} + \bar{a}\cos\theta)\Delta t, y - (\bar{v} + \bar{a}\sin\theta)\Delta t, t). \end{aligned}$$

After some computations, similar to those in Section 2, we obtain the following formulae for the exact solution $\boldsymbol{v}$ of the linearised system at the point $P = (\boldsymbol{x}, t + \Delta t)$. In order to use consistent notation we put $Q := Q_1(\theta)$, $P' := Q_2$ and $\tilde{t} = t + \Delta t - \tau$.

Then we have

$$\rho(\boldsymbol{x}, t+\triangle t) = \rho(P') - \frac{p(P')}{\bar{a}^2} + \frac{1}{2\pi}\int_0^{2\pi}\left[\frac{p(Q)}{\bar{a}^2} - \frac{\bar{\rho}}{\bar{a}}\ (u(Q)\ \cos\theta + v(Q)\ \sin\theta)\right]\ \mathrm{d}\theta$$

$$-\frac{\bar{\rho}}{\bar{a}}\frac{1}{2\pi}\int_0^{2\pi}\int_0^{\triangle t} S(\boldsymbol{x} - (\bar{\boldsymbol{u}} - \bar{a}\boldsymbol{n}(\theta))\tau, \theta, \tilde{t})\ \mathrm{d}\tau\ \mathrm{d}\theta, \tag{3.22}$$

$$u(\boldsymbol{x}, t+\triangle t) = \frac{1}{2\pi}\int_0^{2\pi}\left[-\frac{p(Q)}{\bar{\rho}\bar{a}}\ \cos\theta + (u(Q)\ \cos\theta + v(Q)\ \sin\theta)\ \cos\theta\right]\ \mathrm{d}\theta$$

$$+\frac{1}{2\pi}\int_0^{2\pi}\int_0^{\triangle t}\cos\theta\, S(\boldsymbol{x} - (\bar{\boldsymbol{u}} - \bar{a}\boldsymbol{n}(\theta))\tau, \theta, \tilde{t})\ \mathrm{d}\tau\ \mathrm{d}\theta$$

$$+\frac{1}{2}u(P') - \frac{1}{2\bar{\rho}}\int_0^{\triangle t} p_x(P'(\tilde{t}))\ \mathrm{d}\tau, \tag{3.23}$$

$$v(\boldsymbol{x}, t+\triangle t) = \frac{1}{2\pi}\int_0^{2\pi}\left[-\frac{p(Q)}{\bar{\rho}\bar{a}}\ \sin\theta + (u(Q)\ \cos\theta + v(Q)\ \sin\theta)\sin\theta\right]\ \mathrm{d}\theta$$

$$+\frac{1}{2\pi}\int_0^{2\pi}\int_0^{\triangle t}\sin\theta S(\boldsymbol{x} - (\bar{\boldsymbol{u}} - \bar{a}\boldsymbol{n}(\theta))\tau, \theta, \tilde{t})\ \mathrm{d}\tau\ \mathrm{d}\theta$$

$$+\frac{1}{2}v(P') - \frac{1}{2\bar{\rho}}\int_0^{\Delta t} p_y(P'(\tilde{t}))\ \mathrm{d}\tau, \tag{3.24}$$

$$p(\boldsymbol{x}, t+\triangle t) = \frac{1}{2\pi}\int_0^{2\pi}\left[p(Q) - \bar{\rho}\bar{a}\ (u(Q)\ \cos\theta + v(Q)\ \sin\theta)\right]\ \mathrm{d}\theta$$

$$-\bar{\rho}\bar{a}\frac{1}{2\pi}\int_0^{2\pi}\int_0^{\Delta t} S(\boldsymbol{x} - (\bar{\boldsymbol{u}} - \bar{a}\boldsymbol{n}(\theta))\tau, \theta, \tilde{t})\ \mathrm{d}\tau\ \mathrm{d}\theta, \tag{3.25}$$

where

$$\boldsymbol{x} - (\bar{\boldsymbol{u}} - \bar{a}\boldsymbol{n}(\theta))\tau = (x - (\bar{u} - \bar{a}\cos\theta)\tau,\ y - (\bar{v} - \bar{a}\sin\theta)\tau)$$

and the source term S is given by

$$S(\boldsymbol{x}, \theta, \tilde{t}) := \bar{a}[u_x(\boldsymbol{x}, \theta, \tilde{t})\sin^2\theta - (u_y(\boldsymbol{x}, \theta, \tilde{t}) + v_x(\boldsymbol{x}, \theta, \tilde{t})\sin\theta\cos\theta + v_y(\boldsymbol{x}, \theta, \tilde{t})\cos^2\theta]. \tag{3.26}$$

Approximate evolution operators for the Euler equations.

In our previous papers [12], [13] we have approximated the source term integrals, i.e. the so-called mantle integrals, with respect to time by the rectangle rule, which gives an $\mathcal{O}(\Delta t)$ approximation. As for the wave equation system this led to the reduced stability of the FVEG scheme. Thus the mantle integrals need to be approximated in a better way; and we do this in such a way that each one-dimensional wave is calculated exactly. Using results from Section 2 and the Appendix for the wave equation system we can derive new EG approximate evolution operators for the Euler equations, for which the CFL number is close to a natural stability limit.

Corresponding to (2.18) - (2.20) the approximate evolution operator E_Δ^{const} for *piecewise constant* functions reads:

$$\rho(P) = \rho(P') - \frac{p(P')}{\bar{a}^2} + \frac{1}{2\pi}\int_0^{2\pi}\left[\frac{p(Q)}{\bar{a}^2} - \frac{\bar{\rho}}{\bar{a}}\,\left(u(Q)\,\mathrm{sgn}(\cos\theta) + v(Q)\,\mathrm{sgn}(\sin\theta)\right)\right]\mathrm{d}\theta + \mathcal{O}(\Delta t^2), \tag{3.27}$$

$$u(P) = \frac{1}{2\pi}\int_0^{2\pi}\left[-\frac{p(Q)}{\bar{\rho}\bar{a}}\,\mathrm{sgn}(\cos\theta) + u(Q)\,\left(\tfrac{1}{2} + \cos^2\theta\right) + v(Q)\,\sin\theta\,\cos\theta\right]\mathrm{d}\theta + \mathcal{O}(\Delta t^2), \tag{3.28}$$

$$v(P) = \frac{1}{2\pi}\int_0^{2\pi}\left[-\frac{p(Q)}{\bar{\rho}\bar{a}}\,\mathrm{sgn}(\sin\theta) + u(Q)\,\sin\theta\,\cos\theta + v(Q)\,\left(\tfrac{1}{2} + \sin^2\theta\right)\right]\mathrm{d}\theta + \mathcal{O}(\Delta t^2), \tag{3.29}$$

$$p(P) = \frac{1}{2\pi}\int_0^{2\pi}\left[p(Q) - \bar{\rho}\bar{a}\,\left(u(Q)\,\mathrm{sgn}(\cos\theta) + v(Q)\,\mathrm{sgn}(\sin\theta)\right)\right]\mathrm{d}\theta + \mathcal{O}(\Delta t^2), \tag{3.30}$$

where $Q = (x - \Delta t(\bar{u} - \bar{a}\cos\theta), y - \Delta t(\bar{v} - \bar{a}\sin\theta), t)$, $P' = (x - \Delta t\bar{u}, y - \Delta t\bar{v}, t)$, and $P = (x, y, t + \Delta t)$. Note again that the error $\mathcal{O}(\Delta t^2)$ is obtained if $\nu = 1$, otherwise the approximation error is $\mathcal{O}(\Delta t)$.

Further, the approximate evolution operator E_Δ^{bilin} for continuous *piecewise bilinear* functions is given as follows:

$$\rho(P) = \rho(P') + \frac{1}{4}\int_0^{2\pi}\frac{1}{\bar{a}^2}\left[p(Q) - p(P')\right]\mathrm{d}\theta - \frac{1}{\pi}\int_0^{2\pi}\frac{\bar{\rho}}{\bar{a}}\left[u(Q)\cos\theta + v(Q)\sin\theta\right]\mathrm{d}\theta + \mathcal{O}(\Delta t^2), \tag{3.31}$$

$$u(P) = u(P') - \frac{1}{\pi}\int_0^{2\pi}\frac{p(Q)}{\bar{\rho}\bar{a}}\,\cos\theta\,\mathrm{d}\theta + \frac{1}{4}\int_0^{2\pi}\Big[3\,\left(u(Q)\cos\theta + v(Q)\sin\theta\right)\cos\theta - u(Q) - \tfrac{1}{2}u(P')\Big]\mathrm{d}\theta + \mathcal{O}(\Delta t^2), \tag{3.32}$$

$$v(P) = v(P') - \frac{1}{\pi}\int_0^{2\pi} \frac{p(Q)}{\bar{\rho}\bar{a}}\,\sin\theta\,\mathrm{d}\theta + \frac{1}{4}\int_0^{2\pi} \Big[3\,(u(Q)\cos\theta + v(Q)\sin\theta)\,\sin\theta - v(Q) - \tfrac{1}{2}v(P')\Big]\mathrm{d}\theta + \mathcal{O}(\Delta t^2), \quad (3.33)$$

$$p(P) = p(P') + \frac{1}{4}\int_0^{2\pi} [p(Q) - p(P')]\,\mathrm{d}\theta - \frac{1}{\pi}\int_0^{2\pi} \bar{\rho}\bar{a}\,[u(Q)\cos\theta + v(Q)\sin\theta]\,\mathrm{d}\theta + \mathcal{O}(\Delta t^2). \quad (3.34)$$

It is possible to define a second order FVEG scheme just by using the approximate evolution operator (3.31) - (3.34) and continuous or discontinuous recoveries, R_h^C or R_h^D, respectively. Thus, in the same way as for the wave equation system, we will get the FVEG-A and FVEG-B schemes defined by (3.15) and (3.13), respectively. However, our experience from the wave equation system shows us that the desirable scheme, i.e. the best stability range as well as the best accuracy, is the scheme FVEG-A, which is given by the combination of E_Δ^{const} with E_Δ^{bilin}; cf. (3.16) for the version with a limiter.

4. Numerical experiments. We will present results of several numerical experiments for the linear wave equation system as well as for the nonlinear Euler equations and compare the behaviour of various second order FVEG schemes.
First we refine our notation for the schemes. The FVEG-A is the second order FVEG scheme (3.15), which uses the continuous bilinear recovery R_h^C but is adjusted to maintain the cell average; then we distinguish FVEG-A1 and FVEG-A2 according to whether Simpson's rule or the trapezoidal rule is used for the integration of the edge fluxes. Similarly the FVEG-B1 and FVEG-B2 are those schemes based on the unadjusted operator combination (3.13). Finally, for comparison let FVEG-C be the first order scheme, based on piecewise constants with no recovery and exact evaluation of the edge integrals, given by (3.10) (while FVEG-C1 and FVEG-C2 denote when Simpson's rule or the trapezoidal rule replaces this).
We will also make some comparisons with the second order Lax-Wendroff (rotated Richtmyer) scheme (3.8) and a FVEG scheme based on the earlier operator EG3 studied in [8]-[15], [20].

Problem 1.
We consider the initial value problem for the wave equation system with the initial values

$$\phi(\boldsymbol{x}, 0) = -\frac{1}{c}(\sin 2\pi x + \sin 2\pi y),\ \ u(\boldsymbol{x}, 0) = 0 = v(\boldsymbol{x}, 0).$$

In this case the exact solution is known

$$\phi(\boldsymbol{x}, t) = -\frac{1}{c}\cos 2\pi ct(\sin 2\pi x + \sin 2\pi y), \quad (4.1)$$

$$u(\boldsymbol{x}, t) = \frac{1}{c}\sin 2\pi ct\cos 2\pi x, \quad (4.2)$$

$$v(\boldsymbol{x}, t) = \frac{1}{c}\sin 2\pi ct\cos 2\pi y. \quad (4.3)$$

First we have tested stability ranges of the above schemes on various numerical experiments. The maximum stable CFL numbers $\nu = c\Delta t/h$ that are indicated by the

numerical experiments are as follows: the schemes FVEG-A1 and FVEG-C1 have the stability limits 0.75 and 0.79, respectively; whereas the schemes FVEG-A2 and FVEG-C2 are stable up to 0.96 and 0.99, respectively. We can notice the influence of the Simpson quadrature used for the cell interface integration, which reduces the stablity range. Recall that for the scheme FVEG3 (based on the R_h^D recovery but the earlier EG3 evolution operator) the limit was 0.56.
Next we compare the accuracy of the above FVEG schemes. We take the CFL number $\nu = 0.8$ and an end time $T = 1.0$. In Table 1 the L^2- errors for the second order Lax-Wendroff scheme, the second order wave propagation method of LeVeque computed by the CLAWPACK code [6], and the FVEG schemes with the trapezoidal rule are given for meshes of 20×20, $40\times 40, \ldots, 320\times 320$ cells, together with the experimental order of convergence (EOC) computed from two meshes of sizes N_1 and N_2 as

$$\mathrm{EOC} = \ln \frac{\|\boldsymbol{u}_{N_1}(T) - \boldsymbol{U}^n_{N_1}\|}{\|\boldsymbol{u}_{N_2}(T) - \boldsymbol{U}^n_{N_2}\|} / \ln\left(\frac{N_2}{N_1}\right).$$

Here we have denoted by $\boldsymbol{u}_N(T)$ and by $\boldsymbol{U}^n_N$ the exact and the approximate solutions on a mesh of size N, respectively.
Being in the common stability range the use of the trapezoidal or Simpson's rule for the cell interface integrals gives the same global error for all schemes FVEG-A, B and C. For the first order scheme FVEG-C we can also compare the global error obtained by the scheme with exact edge integrals as well as by means of numerical quadratures, i.e. trapezoidal or Simpson's rule; the error is the same.
In summary, the recommended scheme FVEG-A is roughly five times more accurate than the Lax-Wendroff as well as the LeVeque scheme and twenty-five times more accurate than the scheme FVEG-B that does not preserve cell averages at the recovery stage.
Similar comparisons with a CFL number 0.55 allow the inclusion of the FVEG3 scheme: it is more accurate than (non cell average preserving) FVEG-B but has roughly double the error of FVEG-A.

TABLE 4.1
Accuracy test $T = 1.0$, *CFL* $= 0.8$.

$\|\boldsymbol{u}(T) - \boldsymbol{U}^n\|/N$	A	B	C	LW	CLAW
20	0.074389	1.141908	0.698391	0.297976	0.300450
40	0.014173	0.315654	0.358860	0.073712	0.076641
80	0.003220	0.080285	0.188042	0.018567	0.019062
160	0.000783	0.020136	0.096310	0.004649	0.004649
320	0.000194	0.005038	0.048745	0.001163	0.001163
EOC	**2.0129**	**1.9988**	**0.9824**	**1.9991**	**1.9991**

In Table 2 a comparison of CPU times for the FVEG schemes, the Lax-Wendroff scheme and for the LeVeque scheme (CLAW) is given for a mesh with 80×80 cells. We would like to point out that the higher costs for the second order FVEG schemes are mostly due to the numerical integration along cell interfaces. In the first order scheme FVEG-C the exact integration is done, which reduces the CPU costs. Note however, that no attempt has been made to speed up the code other than the simple loop change. Instead of setting the main loop of the code over cells, we set the

TABLE 4.2
Computational costs in time $T = 1.0$, $CFL = 0.8$.

CPU	A	B	C	LW	CLAW
80	7.39 sec.	7.39 sec.	4.88 sec.	0.26 sec.	5.14 sec.

main loop over vertices of the mesh or over the integration points needed in the flux integrals. In such a way evolution at each vertex is computed just once instead of four times.

Problem 2.
The aim of this experiment is to demonstrate the influence of a nonzero advection velocity on the choice of an appropriate quadrature rule for the flux integration. We consider for the wave equation system with advection the same initial value problem as above. Now the exact solution reads

$$\phi(\boldsymbol{x},t) = -\frac{1}{\bar{a}}\cos 2\pi\bar{a}t(\sin 2\pi(x-\bar{u}t) + \sin 2\pi(y-\bar{v}t)), \tag{4.4}$$

$$u(\boldsymbol{x},t) = \frac{1}{\bar{a}}\sin 2\pi\bar{a}t\cos 2\pi(x-\bar{u}t), \tag{4.5}$$

$$v(\boldsymbol{x},t) = \frac{1}{\bar{a}}\sin 2\pi\bar{a}t\cos 2\pi(y-\bar{v}t), \tag{4.6}$$

where $(\bar{u},\bar{v})$ are constant advection velocities and $\bar{a}$ represents the constant speed of sound, cf. (3.21). We set $\bar{u} = 1.0$, $\bar{v} = 0.5$ and $\bar{a} = 1.0$.
The maximum CFL number

$$\nu = \frac{\Delta t}{h}\max\left(|\bar{u}| + \bar{a}, |\bar{v}| + \bar{a}\right)$$

has been taken 0.7 and the end time $T = 1.0$. We compare the behaviour of the first and second order schemes FVEG-C1, FVEG-C2, FVEG-A1 and FVEG-A2, which use Simpson's and the trapezoidal quadrature for the flux integrals, respectively. In Table 3 the L^2-errors are given for meshes of $20\times 20,\ldots,320\times 320$ cells.
The experiment demonstrates even for this simple test the instability of the FVEG-C2 schemes, which is appearing on the mesh with 320×320 cells. Similarly we see the loss of accuracy of the second order scheme FVEG-A2, which also indicates the instability and would be seen more clearly on a finer mesh. The instability is due to the trapezoidal rule approximation of the flux integrals as was predicted theoretically for a simplified model advection equation in Section 3.2.

Problem 3.
In this example we present the behaviour of our FVEG schemes for the nonlinear Euler equations of gas dynamics. Let us take the well-known Sod-2D test problem with discontinuous initial data

$$\begin{aligned} \rho = 1, \quad u = 0, \quad v = 0, \quad p = 1, \quad \|\boldsymbol{x}\| < 0.4 \\ \rho = 0.125, \quad u = 0, \quad v = 0, \quad p = 0.1, \quad \text{else.} \end{aligned}$$

TABLE 4.3

Accuracy of the FVEG schemes using Simpson's and the trapezoidal rule for the wave equation system with advection, $T = 1.0$, $CFL = 0.7$.

$\|\boldsymbol{u}(T) - \boldsymbol{U}^n\|/N$	A1	A2	C1	C2
20	0.138311	0.138311	1.036531	1.036531
40	0.026628	0.026628	0.649852	0.649852
80	0.005990	0.005990	0.370421	0.370421
160	0.001455	0.001455	0.198350	0.198350
320	0.000361	0.000498	0.102650	2.395565
EOC	**2.0109**	**1.5468**	**0.9503**	–

We consider this initial-value problem as a cylindrical explosion problem. The computational domain is a square $[-1,1]\times[-1,1]$. The mesh is uniform square and initial data are implemented by taking the integral average on each cell, i.e. by projecting them onto a piecewise constant function in S_h^0. As pointed out by Toro in [21] this avoids the formation of small amplitude waves created at early times by a staircase configuration of the data. We set the CFL number to 0.7 and take a mesh with 400 $\times$ 400 cells.

The solution exhibits a circular shock travelling away from the centre, a circular contact discontinuity travelling in the same direction and a circular rarefaction wave travelling towards the origin at $(0,0)$. Within the rarefaction fan a secondary shock is created, it travels inwards and focuses at the origin creating a peak in pressure and density at time $T = 1.7$. In Figure 3 we have plotted three-dimensional graphs of density at $T = 0.2$ and $T = 1.7$ computed by the second order FVEG-A1 scheme. Note that small oscillations at time $T = 1.7$ are caused by partially reflected boundary waves; a similar phenomenon can also be experienced with the LeVeque scheme. To model absorbing boundary conditions we have used just simple second order extrapolation of all physical variables at the boundary. In [16], [20] other suitable techniques for approximation of boundary conditions were studied.

Further, we have compared the numerical solutions computed by the FVEG-A1 and FVEG-A2 schemes, i.e. using Simpson's rule and the trapezoidal approximation of the edge integrals, respectively; in Figures 4 and 5 are given the isolines of density, velocity, and pressure at time $T = 0.2$. The results confirm that the trapezoidal rule is not appropriate for problems with arbitrary advection velocities, i.e. $\bar{u} \neq \bar{v}$. Note that in order to supress typical over-/undershoots on discontinuities we used the minmod limiter to control the slopes; see our previous paper [13] for a precise definition as well as for further experiments and comparisons with other schemes. Figure 4 illustrates good multidimensional resolution of all significant structures of the solution.

5. Conclusions. In this paper we have derived new genuinely multidimensional finite volume evolution Galerkin schemes, which are based on the use of a multidimensional approximate evolution operator. The method consists of two steps and couples a finite volume formulation with an approximate evolution Galerkin operator. The latter is constructed using the bicharacteristics of the multidimensional hyperbolic system, such that all of the infinitely many directions of wave propagation are taken into account. In the first step a recovered (or reconstructed) approximate solu-

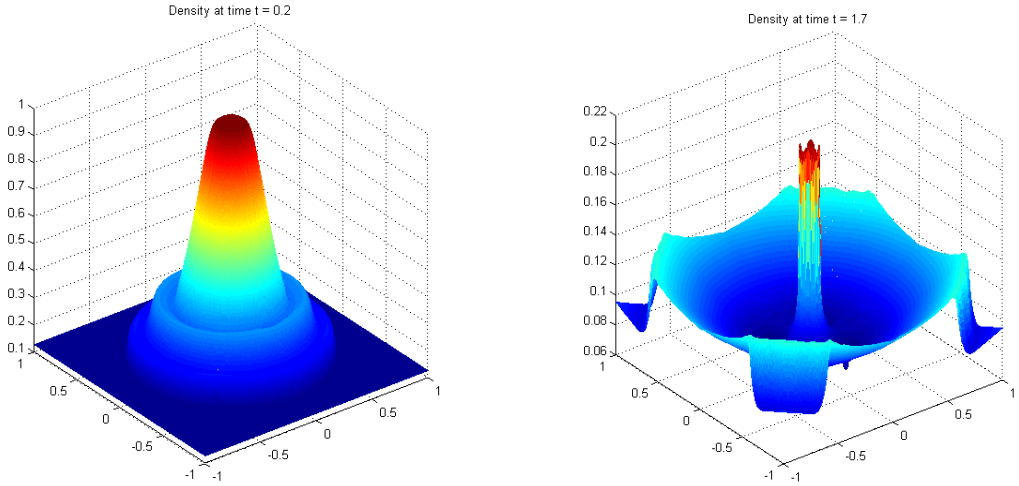

FIG. 4.1. *Cylindrical explosion, graphs of density at* $T = 0.2$ *and* $T = 1.7$. *Solution obtained by the FVEG-A1 scheme on a* 400×400 *mesh.*

tion is evolved by the approximate evolution operator, and fluxes along cell edges are calculated. In the second step the finite volume update is done.
We have derived new approximate evolution operators, E_Δ^{bilin} and E_Δ^{const}, which work with continuous piecewise bilinear or piecewise constant functions, respectively. The operators are constructed in such a way that any one-dimensional planar wave, oriented with the mesh, is calculated exactly. As a result, the stability ranges of the FVEG schemes are improved considerably and the stability limits are close to the natural limits of CFL $= 1$. Moreover, if the slopes of the approximate solution are evolved by means of E_Δ^{bilin} and constant parts are corrected by means of E_Δ^{const}, in order to preserve cell averages at the recovery stage, the accuracy of the FVEG scheme is also improved considerably to yield our preferred scheme FVEG-A. Furthermore in the case of advected characteristic cones it is shown to be important to use Simpson's rule to evaluate the edge fluxes, giving the scheme FVEG-A1.
Numerical experiments for the linear wave equation system as well as for the nonlinear Euler equations of gas dynamics confirm the improved accuracy and stability of new FVEG schemes, as well as good multidimensional resolution. Further comparisons with commonly known schemes were presented in [13] .

A. Appendix: Exact mantle integrals for the evolution operator of the system wave equation. For one-dimensional data, the solution of the wave equation can be written down explicitly and substituted into the mantle integrals occurring in the formulae (2.14) - (2.17). Exact evaluation of these integrals for discontinuous, piecewise linear data then provides a guide to the choice of quadrature to be used for more general two-dimensional data.
We begin with the piecewise constant initial data (2.12) and the resulting exact solution (2.13). Suppose this is substituted in the evolution operator formulae (2.14) - (2.15) to give the solution at the origin after one time step; thus

$$\phi(0,0,\Delta t) = \frac{1}{2\pi}\int_0^{2\pi} [\phi_Q - u_Q \cos\theta]\, \mathrm{d}\theta - \frac{1}{2\pi}\int_0^{\Delta t}\frac{1}{\tau}\int_0^{2\pi} u_{Q'}\cos\theta \mathrm{d}\theta\, \mathrm{d}\tau, \qquad \text{(A.1)}$$

where $Q(\theta) = (c\Delta t\cos\theta, c\Delta t\sin\theta, 0)$ and $Q' = (c\tau\cos\theta, c\tau\sin\theta, \Delta t - \tau)$. For these

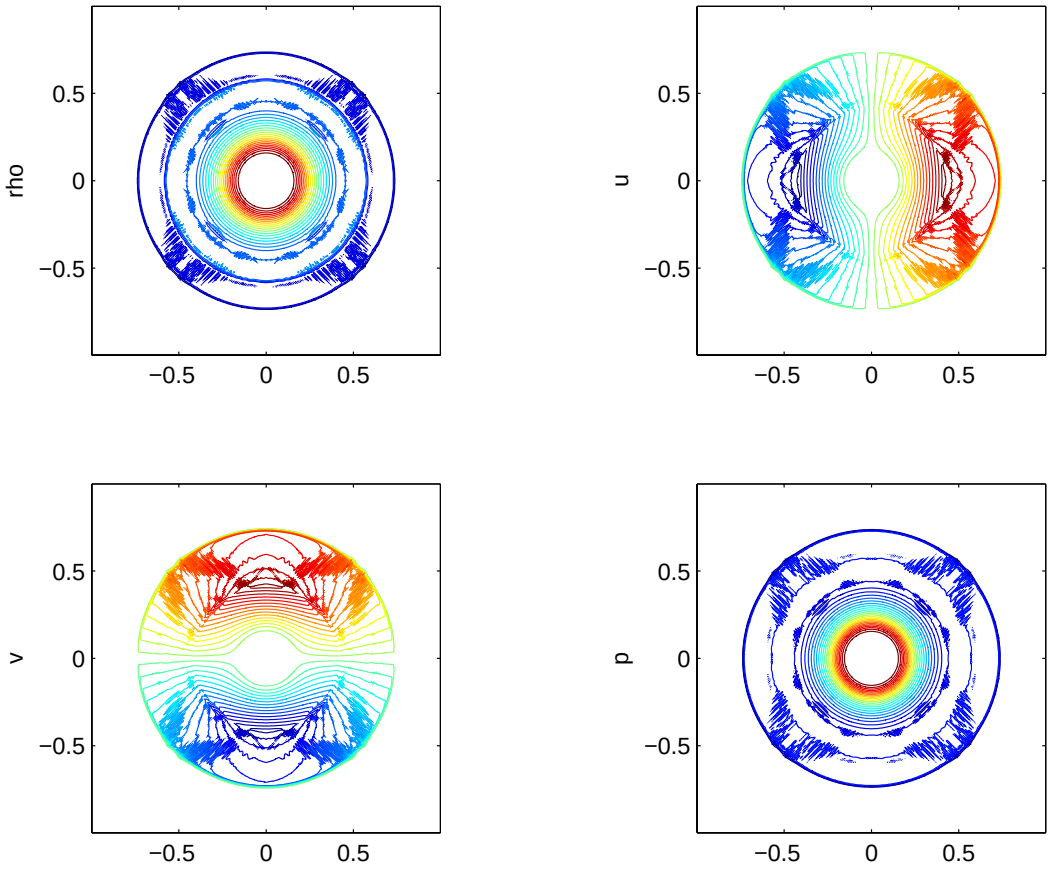

FIG. 4.2. *Cylindrical explosion, isolines of the solution obtained by the FVEG-A2 scheme with the trapezoidal rule at $T = 0.2$ on a 400×400 mesh: the plots show density rho, velocities (u,v) and pressure p.*

data, the first integral gives

$$\frac{1}{2\pi}\int_0^{2\pi} [\phi_Q - u_Q \cos\theta]\,\mathrm{d}\theta = \frac{1}{2}\left(\phi^+ + \phi^-\right) - \frac{1}{\pi}\left(u^+ - u^-\right). \tag{A.2}$$

In the second integral over the mantle $u_{Q'}$ is constant, independently of θ, unless $\tau > \Delta t - \tau$, i.e. $\tau > \frac{1}{2}\Delta t$; indeed, there is cancellation between the left and right of the origin unless $\tau|\cos\theta| > \Delta t - \tau$. With $\bar\theta$ given by $\tau\cos\bar\theta = \Delta t - \tau$, so that $\mathrm{d}\tau/\tau = \sin\bar\theta\mathrm{d}\bar\theta/(1+\cos\bar\theta)$, the integral therefore becomes

$$\frac{1}{2\pi}\int_0^{\Delta t}\frac{1}{\tau}\int_0^{2\pi} u_{Q'}\cos\theta\,\mathrm{d}\theta\mathrm{d}\tau = \frac{1}{2\pi}\int_{\frac{1}{2}\Delta t}^{\Delta t}\frac{1}{\tau}(u^+ - u^-)2\sin\bar\theta\,\mathrm{d}\tau \tag{A.3}$$

$$= \frac{1}{\pi}(u^+ - u^-)\int_0^{\pi/2}\frac{\sin^2\bar\theta}{1+\cos\bar\theta}\,\mathrm{d}\bar\theta = \frac{1}{\pi}(u^+ - u^-)\left(\frac{\pi}{2} - 1\right).$$

Hence the exact solution is reproduced through exactly integrating the two integrals, that is

$$\begin{aligned}\phi(0,0,\Delta t) &= \frac{1}{2}(\phi^+ + \phi^-) - \frac{1}{\pi}(u^+ - u^-) - \left(\frac{1}{2} - \frac{1}{\pi}\right)(u^+ - u^-)\\ &= \frac{1}{2}(\phi^+ + \phi^-) - \frac{1}{2}(u^+ - u^-).\end{aligned} \tag{A.4}$$

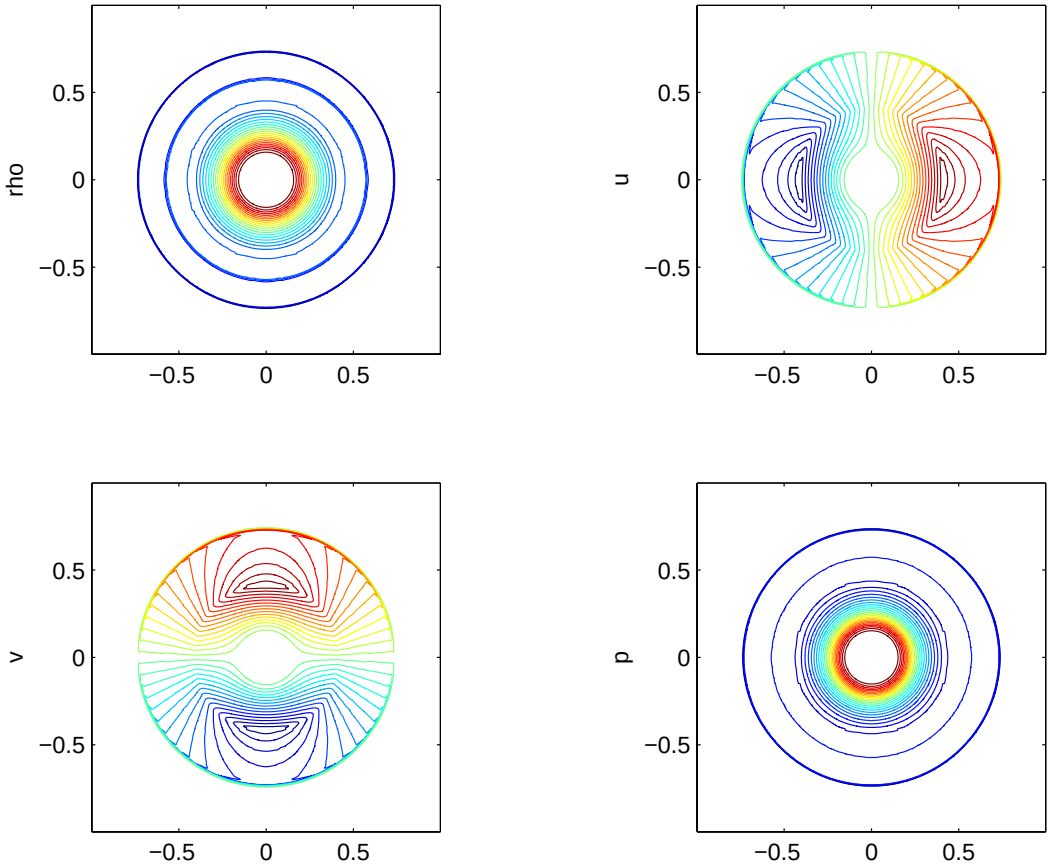

FIG. 4.3. *Cylindrical explosion, isolines of the solution obtained by the FVEG-A1 scheme with Simpson's rule at $T = 0.2$ on a 400×400 mesh: the plots show density rho, velocities (u,v) and pressure p.*

It should be noted that the combined integral over u on the right can be written as

$$\frac{u^+}{2\pi}\int_{-\pi/2}^{\pi/2}\left[\cos\theta + \frac{\sin^2\theta}{1+\cos\theta}\right]\mathrm{d}\theta \equiv \frac{u^+}{2\pi}\int_{-\pi/2}^{\pi/2}\mathrm{d}\theta. \tag{A.5}$$

It is this form that leads to the approximate evolution operator for piecewise constant functions on a general mesh that is given in (2.18) - (2.20); it motivates the use of

$$\frac{1}{2\pi}\int_0^{2\pi} u_Q\,\mathrm{sgn}(\cos\theta)\,\mathrm{d}\theta \equiv \frac{1}{2}\left(u^+ - u^-\right)$$

to combine the u-integrals in (A.2) and (A.3), and hence give an approximation that is equivalent to the corresponding terms in (A.1).

Next, in one dimension, the update for u should be the same as that for ϕ; however, we use the general two-dimensional formula of (2.15), together with (2.17), to give for

the solution after one step

$$u(0,0,\Delta t) = \frac{1}{2\pi}\int_0^{2\pi}[-\phi_Q\cos\theta + u_Q\cos^2\theta]\mathrm{d}\theta + \frac{1}{2}u_{P'} + \frac{1}{2\pi}\int_0^{\Delta t}\frac{1}{\tau}\int_0^{2\pi}[u_{Q'}\cos 2\theta - \phi_{Q'}\cos\theta]\,\mathrm{d}\theta\mathrm{d}\tau \quad \text{(A.6)}$$

We see from this that the dependence on ϕ_Q and $\phi_{Q'}$ is exactly the same as that on u_Q and $u_{Q'}$ in the formula (A.1) for $\phi(0,0,\Delta t)$. Also, the integral of $u_{Q'}\cos 2\theta$ gives no contribution from these data; and $u_{P'}$ should be interpreted as the integral average of u_Q. We then reproduce the exact formula for $u(0,0,\Delta t)$ to match that for $\phi(0,0,\Delta t)$. So again this leads to the approximate evolution operator for $u(P)$ that is given in (2.18) - (2.20).

Now let us consider the continuous linear initial data given by (2.21), which results in the exact solution (2.22). We again substitute the latter in the evolution operator formulae (2.14) - (2.17) and carry out the integrals over the cone base and mantle exactly. From (A.1) with these data the first integral is very simple, giving

$$\frac{1}{2\pi}\int_0^{2\pi}[\phi_Q - u_Q\cos\theta]\,\mathrm{d}\theta = \frac{1}{2\pi}\int_{-\pi/2}^{\pi/2}\left(\phi^R - u^R\cos\theta\right)c\Delta t\cos\theta\mathrm{d}\theta = c\Delta t\left(\frac{1}{\pi}\phi^R - \frac{1}{4}u^R\right), \quad \text{(A.7)}$$

instead of (A.2).

The mantle integral is more complicated, because of the change of solution form along the line $x = c\tilde{t} = c(\Delta t - \tau)$, which cuts the mantle at $\theta = \bar{\theta}$ (given by $\tau\cos\bar{\theta} = \Delta t - \tau$ as used in (A.3)) if $\tau \geq \frac{1}{2}\Delta t$. We therefore first prove a more general result which we can utilize later.

LEMMA A.1. *For the 1D wave equation solution*

$$\phi(x,t) = f(x-ct) + g(x+ct), \quad u(x,t) = f(x-ct) - g(x+ct), \quad \text{(A.8)}$$

where $f, g \in H^1(\mathbb{R})$, the mantle integrals in (2.14) and (2.15) (evaluated at the origin) are given by

$$\frac{1}{2\pi}\int_0^{\Delta t}\frac{1}{\tau}\int_0^{2\pi} f_{Q'}\begin{pmatrix}\cos\theta\\ \cos 2\theta\end{pmatrix}d\theta\,d\tau = \begin{pmatrix}-1\\ 1/2\end{pmatrix}f(-c\Delta t) + \frac{1}{2\pi}\int_0^{2\pi}\begin{pmatrix}1\\ \cos\theta\end{pmatrix}f(c\Delta t\cos\theta)(1-\cos\theta)\,d\theta, \quad \text{(A.9)}$$

$$\frac{1}{2\pi}\int_0^{\Delta t}\frac{1}{\tau}\int_0^{2\pi} g_{Q'}\begin{pmatrix}\cos\theta\\ \cos 2\theta\end{pmatrix}d\theta\,d\tau = \begin{pmatrix}1\\ 1/2\end{pmatrix}g(c\Delta t) - \frac{1}{2\pi}\int_0^{2\pi}\begin{pmatrix}1\\ \cos\theta\end{pmatrix}g(c\Delta t\cos\theta)(1+\cos\theta)\,d\theta. \quad \text{(A.10)}$$

Proof. For $f_{Q'}\cos\theta$ the left-hand side equals

$$\begin{aligned}
&\frac{1}{2\pi}\int_0^{\Delta t}\frac{1}{\tau}\int_0^{2\pi} f(c\tau\cos\theta - c(\Delta t-\tau))\cos\theta \mathrm{d}\theta\mathrm{d}\tau \\
&\quad= \frac{1}{2\pi}\int_0^{\Delta t}\frac{1}{\tau}\left\{[\sin\theta f(\cdot)]_0^{2\pi} + \int_0^{2\pi} c\tau\sin^2\theta f'(c(1+\cos\theta)\tau - c\Delta t)\mathrm{d}\theta\right\}\mathrm{d}\tau \\
&\quad= \frac{1}{2\pi}\int_0^{2\pi} c\sin^2\theta\left\{\int_0^{\Delta t} f'(\tau)\mathrm{d}\tau = \frac{f(c\Delta t\cos\theta) - f(-c\Delta t)}{c(1+\cos\theta)}\right\}\mathrm{d}\theta \\
&\quad= \frac{1}{2\pi}\int_0^{2\pi}(1-\cos\theta)\left[f(c\Delta t\cos\theta) - f(-c\Delta t)\right]\mathrm{d}\theta \\
&\quad= -f(-c\Delta t) + \frac{1}{2\pi}\int_0^{2\pi} f(c\Delta t\cos\theta)(1-\cos\theta)\mathrm{d}\theta,
\end{aligned}$$

as given in (A.9).
For $f_{Q'}\cos 2\theta$, after integrating $\cos 2\theta$ to give $\frac{1}{2}\sin 2\theta = \sin\theta\cos\theta$, we obtain instead on the third line

$$\begin{aligned}
&\frac{1}{2\pi}\int_0^{2\pi} c\sin^2\theta\cos\theta\left\{\int_0^{\Delta t} f'(\tau)\mathrm{d}\tau = \frac{f(c\Delta t\cos\theta) - f(-c\Delta t)}{c(1+\cos\theta)}\right\}\mathrm{d}\theta \\
&\qquad= \frac{1}{2\pi}\int_0^{2\pi}(1-\cos\theta)\cos\theta\left[f(c\Delta t\cos\theta) - f(-c\Delta t)\right]\mathrm{d}\theta \\
&\qquad= \frac{1}{2}f(-c\Delta t) + \frac{1}{2\pi}\int_0^{2\pi} f(c\Delta t\cos\theta)(1-\cos\theta)\cos\theta\mathrm{d}\theta,
\end{aligned}$$

as given in (A.9).
For the left-moving waves, $g_{Q'}\cos m\theta$ gives with the change $\theta \longrightarrow \pi+\theta$ and $g(\psi) \longrightarrow f(-\psi)$

$$\begin{aligned}
&\frac{1}{2\pi}\int_0^{\Delta t}\frac{1}{\tau}\int_0^{2\pi} g(c\tau\cos\theta + c(\Delta t-\tau))\cos m\theta\,\mathrm{d}\theta\mathrm{d}\tau \\
&\quad= \frac{1}{2\pi}\int_0^{\Delta t}\frac{1}{\tau}\int_0^{2\pi} g(-c\tau\cos\theta + c(\Delta t-\tau))(-1)^m\cos m\theta\mathrm{d}\theta\,\mathrm{d}\tau \\
&\quad= \frac{(-1)^m}{2\pi}\int_0^{\Delta t}\frac{1}{\tau}\int_0^{2\pi} f(c\tau\cos\theta - c(\Delta t-\tau))\cos m\theta\mathrm{d}\theta\,\mathrm{d}\tau \qquad \text{(A.11)}
\end{aligned}$$

to which (A.9) can be applied; then the changes back, $\theta \longrightarrow \pi+\theta$ and $f(\psi) \longrightarrow g(-\psi)$, gives the result in terms of $g(\cdot)$ as (A.10). □

For the initial data (2.21) we write the solution (2.22) at Q' in the form

$$\phi_{Q'} = \tfrac{1}{2}(\phi^R + u^R)(x - c\tilde{t})^+ + \tfrac{1}{2}(\phi^R - u^R)(x + c\tilde{t})^+ \qquad \text{(A.12)}$$
$$u_{Q'} = \tfrac{1}{2}(\phi^R + u^R)(x - c\tilde{t})^+ - \tfrac{1}{2}(\phi^R - u^R)(x + c\tilde{t})^+, \qquad \text{(A.13)}$$

where $x = \tau\cos\theta$ and $\tilde{t} = \Delta t - \tau$. Now we can use the lemma to compute the mantle integral in the ϕ update of (2.14) or (A.1): from $f(x) \equiv x^+ \equiv \max(x,0)$, so that

$(\cos\theta)^+$ gives a contribution only if $\theta \in]-\pi/2, \pi/2[$, we get

$$\frac{1}{2\pi}\int_0^{\Delta t}\frac{1}{\tau}\int_0^{2\pi}(x-c\tilde{t})^+_{Q'}\cos\theta \mathrm{d}\theta\mathrm{d}\tau = \frac{c\Delta t}{2\pi}\int_{-\pi/2}^{\pi/2}\cos\theta(1-\cos\theta)\mathrm{d}\theta = c\Delta t\left(\frac{1}{\pi}-\frac{1}{4}\right); \tag{A.14}$$

and from $g(x) \equiv x^+$ we get

$$\frac{1}{2\pi}\int_0^{\Delta t}\frac{1}{\tau}\int_0^{2\pi}(x+c\tilde{t})^+_{Q'}\cos\theta \mathrm{d}\theta\mathrm{d}\tau = c\Delta t - \frac{c\Delta t}{2\pi}\int_{-\pi/2}^{\pi/2}\cos\theta(1+\cos\theta)\mathrm{d}\theta = c\Delta t\left(\frac{3}{4}-\frac{1}{\pi}\right). \tag{A.15}$$

Putting these together from (A.11), the mantle integral becomes in this case

$$\begin{aligned}\frac{1}{2\pi}\int_0^{\Delta t}\frac{1}{\tau}\int_0^{2\pi}u_{Q'}\cos\theta\mathrm{d}\theta\mathrm{d}\tau &= \frac{1}{2}(\phi^R+u^R)c\Delta t\left(\frac{1}{\pi}-\frac{1}{4}\right)-\frac{1}{2}\left(\phi^R-u^R\right)c\Delta t\left(\frac{3}{4}-\frac{1}{\pi}\right)\\ &= c\Delta t\left[\left(\frac{1}{\pi}-\frac{1}{2}\right)\phi^R+\frac{1}{4}u^R\right].\end{aligned} \tag{A.16}$$

Subtracting this from (A.7) then yields for (A.1) the result

$$\phi(0,0,\Delta t) = \tfrac{1}{2}c\Delta t(\phi^R - u^R), \tag{A.17}$$

which is in agreement with the exact solution given by (2.22).
Thus in order to modify the cone base integral, giving (A.7), so that it incorporates the effect of the mantle integral, given by subtracting (A.16), we need to make two changes: firstly, the term arising from integrating $u_Q\cos\theta$ needs to be doubled, which has the same effect as applying the rectangle rule to approximate the mantle integral; and secondly, the term from ϕ_Q needs to be split into the two parts $\phi_{P'}+(\phi_Q-\phi_{P'})$, and that from the latter must be multiplied by $\pi/2$. This leads to the update formula (2.23) to approximate (2.14) in the case of continuous data.
For the update of u, the cone base terms with the data of (2.21) give

$$\begin{aligned}\frac{1}{2}u_{P'}+\frac{1}{2\pi}\int_0^{2\pi}[u_Q\cos^2\theta-\phi_Q\cos\theta]\mathrm{d}\theta &= \frac{c\Delta t}{2\pi}\int_{-\pi/2}^{\pi/2}(u^R\cos^3\theta-\phi^R\cos^2\theta)\mathrm{d}\theta\\ &= c\Delta t\left(\frac{2}{3\pi}u^R-\frac{1}{4}\phi^R\right).\end{aligned} \tag{A.18}$$

The mantle term in $\phi_{Q'}\cos\theta$, introduced in (2.17), gives as in (A.16)

$$\frac{1}{2\pi}\int_0^{\Delta t}\frac{1}{\tau}\int_0^{2\pi}\phi_{Q'}\cos\theta\mathrm{d}\theta\mathrm{d}\tau = c\Delta t\left[\left(\frac{1}{\pi}-\frac{1}{2}\right)u^R+\frac{1}{4}\phi^R\right]. \tag{A.19}$$

Finally, the mantle term in $u_Q\cos 2\theta$ is obtained from (A.9) and (A.10), as in (A.12) - (A.16), giving

$$\begin{aligned}\frac{1}{2\pi}\int_0^{\Delta t}\frac{1}{\tau}\int_0^{2\pi}u_{Q'}\cos 2\theta\,\mathrm{d}\theta\mathrm{d}\tau &= \frac{1}{2}(\phi^R+u^R)\frac{c\Delta t}{2\pi}\int_{-\pi/2}^{\pi/2}\cos^2\theta(1-\cos\theta)\mathrm{d}\theta\\ &\quad -\frac{1}{2}(\phi^R-u^R)\left[\frac{1}{2}c\Delta t-\frac{c\Delta t}{2\pi}\int_{-\pi/2}^{\pi/2}\cos^2\theta(1+\cos\theta)\mathrm{d}\theta\right]\\ = \frac{1}{2}(\phi^R+u^R)c\Delta t\left(\frac{1}{4}-\frac{2}{3\pi}\right)-\frac{1}{2}\left(\phi^R-u^R\right)c\Delta t\left(\frac{1}{4}-\frac{2}{3\pi}\right) &= \left(\frac{1}{4}-\frac{2}{3\pi}\right)c\Delta t u^R\end{aligned} \tag{A.20}$$

Thus the combination of (2.15) and (2.17) gives the update from (A.18), (A.19) and (A.20) as

$$u(0,0,\Delta t) = c\Delta t \left[u^R \left(\frac{2}{3\pi} - \frac{1}{\pi} + \frac{1}{2} + \frac{1}{4} - \frac{2}{3\pi} \right) + \phi^R(-\frac{1}{4} - \frac{1}{4}) \right]$$
$$= c\Delta t \left[\left(\frac{3}{4} - \frac{1}{\pi} \right) u^R - \frac{1}{2}\phi^R \right]. \qquad \text{(A.21)}$$

Unlike (A.17), this is not in agreement with the exact solution given by (2.22). This is because of the approximation made in (2.17): for the present data, the left-hand side of (2.17) can be calculated exactly to give $\frac{1}{4}c\Delta t(\phi^R - u^R)$; if (A.19) is replaced by this expression we recover the exact solution.

Finally, then, to deduce the update formula (2.24) to approximate (2.15) and (2.17), we first need to double the term arising from $\phi_Q \cos\theta$. In the same way we add a term $u_Q \cos 2\theta$, corresponding to applying the rectangle rule to the mantle term $u_{Q'} \cos 2\theta$, to the cone base integral of $u_Q \cos^2\theta$ to give $u_Q(3\cos^2\theta - 1)$. Then we split u_Q into $u_{P'} + (u_Q - u_{P'})$ and multiply the term arising from the latter by $\pi/2$. This leads to (2.24).

In this way we have completed the derivation of update formulae (2.23) - (2.25), based on only the cone base values, to approximate the formulae (2.14) - (2.17) in such a way as to be exact for continuous, piecewise linear, one-dimensional grid-aligned data. Note that there is a close similarity between the treatment of the ϕ update and the u update, except that the $\cos^2\theta$ coefficient is introduced so as to respect the integrity of the term $u\cos\theta + v\sin\theta$, whose integral around the perimeter of the cone base equals the divergence of the velocity field averaged over the base.

Acknowledgements.
This research was supported by the VolkswagenStiftung Agency, by the Deutsche Forschungsgemeinschaft Grant No. Wa 633/6-2 and partially by the European network HYKE, funded by the EC as contract HPRN-CT-2002-00282. Authors gratefully acknowledge these supports.

REFERENCES

[1] T.J. Barth. Aspects of unstructured grids and finite-volume solvers for the Euler and Navier-Stokes equations, *AGARD Report* 787, 6.1-6.61, 1992.

[2] M. Ben-Artzi, J. Falcovitz. A Second-order Godunov-type scheme for compressible fluid dynamics, *J. Comput. Phys.*, 55:1-32, 1984.

[3] R. Courant, D. Hilbert. *Methods of Mathematical Physics*, Interscience Publishers, 1962.

[4] H. Deconinck, P. Roe, R. Struijs. A multidimensional generalization of Roe's flux difference splitter for the Euler equations, *Comput. Fluids*, 22(2-3):215-222, 1993.

[5] T. Kröger, S. Noelle, S. Zimmermann. On the connection between some Riemann-solver free approaches to the approximation of multi-dimensional systems of hyperbolic consrvaton laws, RWTH-Preprint Nr. 228, submitted, 2003.

[6] R.J. LeVeque. Wave propagation algorithms for multi-dimensional hyperbolic systems, *J. Comp. Phys.*, 131:327–353, 1997.

[7] R.J. LeVeque. *Finite Volume Methods for Hyperbolic Problems,* Cambridge University Press, 2002.

[8] M. Lukáčová - Medviďová, K.W. Morton, G. Warnecke. Evolution Galerkin methods for hyperbolic systems in two space dimensions, *Math. Comp.*, 69:1355–1384, 2000.

[9] M. Lukáčová-Medviďová, K. W. Morton, G. Warnecke. Finite volume evolution Galerkin methods for multidimensional hyperbolic problems, *Proceedings of the Finite Volumes for Complex Applications (ed. R. Vilsmeier et.al.)*, Hermès, 289-296, 1999.

[10] M. Lukáčová - Medviďová, K.W. Morton, G. Warnecke. High-resolution finite volume evolution Galerkin schemes for multidimensional conservation laws, *Proceedings of ENUMATH'99*, World Scientific Publishing Company, Singapore, 1999.

[11] M. Lukáčová - Medviďová, K.W. Morton, G. Warnecke. On high-resolution finite volume evolution Galerkin schemes for genuinely multidimensional hyperbolic conservation laws, *Proceedings of the European Congress on Computational Methods in Applied Sciences and Engineering*, ECCOMAS 2000, 11.-14.9.2000, Barcelona, Spain.

[12] M. Lukáčová-Medviďová, K.W. Morton, G. Warnecke. Finite volume evolution Galerkin methods for Euler equations of gas dynamics, *Int. J. Numer. Meth. Fluids*, 40:425–434, 2002.

[13] M. Lukáčová - Medviďová, J. Saibertová, G. Warnecke. Finite volume evolution Galerkin methods for nonlinear hyperbolic systems, *J. Comp. Phys.*, 183:533–562, 2002.

[14] M. Lukáčová - Medviďová, J. Saibertová. Genuinely multidimensional evolution Galerkin schemes for the shallow water equations, *Numerical Mathematics and Advanced Applications* (eds. Brezzi et al.), 145–149, Springer, 2003.

[15] M. Lukáčová - Medviďová, G. Warnecke. Lax-Wendroff type second order evolution Galerkin methods for multidimensional hyperbolic systems, *East-West J. Num. Math.*, 8(2):127–152, 2000.

[16] M. Lukáčová - Medviďová, G. Warnecke, Y. Zahaykah. On the boundary conditions for EG-methods applied to the two-dimensional wave equation systems, *accepted to ZAMM*, 2003.

[17] K.W. Morton. On the analysis of finite volume methods for evolutionary problems, *SIAM J. Numer. Anal.*, 35(6):2195-2222, 1998.

[18] K.W. Morton. Discretisation of unsteady hyperbolic conservation laws, *SIAM J. Numer. Anal.*, 39(5):1556-1597, 2001.

[19] K.W. Morton, P. Roe. Vorticity-preserving Lax-Wendroff-type schemes for the system of wave equation, *SIAM J.Sci.Comput.*, 23(1):170-192, 2001.

[20] Y. Zahaykah. Evolution Galerkin Schemes and Discrete Boundary Conditions for Multidimensional First Order Systems, *Dissertation*, University of Magdeburg, 2001.

[21] E.F. Toro. *Riemann Solvers and Numerical Methods for Fluid Dynamics, A Practical Introduction,* Springer, 1999.